

## Comparison of different numerical modelling approaches for the assessment of the out-of-plane behaviour of two-leaf stone masonry walls

Murano, Antonio; Mehrotra, Anjali; Ortega, Javier; Rodrigues, Hugo; Vasconcelos, Graça

**DOI**

[10.1016/j.engstruct.2023.116466](https://doi.org/10.1016/j.engstruct.2023.116466)

**Publication date**

2023

**Document Version**

Final published version

**Published in**

Engineering Structures

**Citation (APA)**

Murano, A., Mehrotra, A., Ortega, J., Rodrigues, H., & Vasconcelos, G. (2023). Comparison of different numerical modelling approaches for the assessment of the out-of-plane behaviour of two-leaf stone masonry walls. *Engineering Structures*, 291, Article 116466. <https://doi.org/10.1016/j.engstruct.2023.116466>

**Important note**

To cite this publication, please use the final published version (if applicable). Please check the document version above.

**Copyright**

Other than for strictly personal use, it is not permitted to download, forward or distribute the text or part of it, without the consent of the author(s) and/or copyright holder(s), unless the work is under an open content license such as Creative Commons.

**Takedown policy**

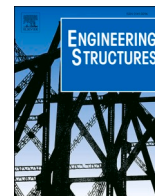
Please contact us and provide details if you believe this document breaches copyrights. We will remove access to the work immediately and investigate your claim.

***Green Open Access added to TU Delft Institutional Repository***

***'You share, we take care!' - Taverne project***

**<https://www.openaccess.nl/en/you-share-we-take-care>**

Otherwise as indicated in the copyright section: the publisher is the copyright holder of this work and the author uses the Dutch legislation to make this work public.



# Comparison of different numerical modelling approaches for the assessment of the out-of-plane behaviour of two-leaf stone masonry walls

Antonio Murano<sup>a,\*</sup>, Anjali Mehrotra<sup>b</sup>, Javier Ortega<sup>c</sup>, Hugo Rodrigues<sup>d</sup>, Graça Vasconcelos<sup>a</sup>

<sup>a</sup> ISISE, Department of Civil Engineering, University of Minho, Guimarães, Campus de Azurém, 4800-058 Guimarães, Portugal

<sup>b</sup> Faculty of Civil Engineering and Geosciences, Department of Mechanics, Management & Design (3Md), Delft University of Technology, Stevinweg 1, 2628 CN Delft, The Netherlands

<sup>c</sup> Institute for Physical and Information Technologies (ITEFI) Leonardo Torres Quevedo, Consejo Superior de Investigaciones Científicas (CSIC), C/Serrano 144, 28006 Madrid, Spain

<sup>d</sup> RISCO, Civil Engineering Department, University of Aveiro, Campus Universitario de Santiago, 3810-193 Aveiro, Portugal

## ARTICLE INFO

### Keywords:

Two-leaf stone masonry walls  
FE micro-modelling  
FE macro-modelling, discrete element method  
Out-of-plane  
Material properties

## ABSTRACT

This work compares the ability of different numerical modelling approaches to simulate the out-of-plane behaviour of two-leaf stone masonry walls with different masonry bond configurations: an irregular drystone stone masonry wall and a masonry wall with roughly cut regular stone units. Finite element modelling, considering both a micro and macro-modelling approach, and the distinct element method have been compared in this study, which intends to (i) provide an insight regarding parameter estimation and the calibration procedure for each modelling approach considered; (ii) highlight their pros and cons of the selected modelling strategies; (iii) further expand the existing literature addressing the numerical modelling of two-leaf stone masonry walls.

## 1. Introduction

Masonry is a composite material made of units (natural or manmade) arranged in space usually following a regular pattern characterised by a succession of horizontal overlapping layers which are staggered to avoid the formation of continuous vertical joints. Ideally, the presence of mortar (made of fine aggregate, sand, water, air and/or hydraulic lime binders) should ensure masonry structures with a monolithic behaviour. In the case of dry-stone masonry, no mortar is present, and the units are stacked on top of each other trying to achieve a good interlock to provide an effective structural stability.

A significant part of the existing worldwide building stock consists of ordinary and historical masonry buildings (churches, temples, fortresses, etc.) [1].

Indeed, historical masonry buildings are often the result of a non-engineered building practice rooted in practical expertise developed by craftsmen over the centuries and successively codified as rules of thumb, which are essentially an array of techniques consistently detected in historical constructions.

Therefore, when it comes to assessing the structural performance of

historical masonry buildings, there are some key aspects that need to be considered, such as the geometrical configuration of masonry bond and the uncertainty related to the estimation of mechanical properties. Inevitably, qualitative, and quantitative features of masonry constructions need to be examined in order to provide an accurate estimation of the overall structural behaviour [2].

The study of qualitative aspects concerning masonry constructions often deals with the analysis and classification of collapse mechanisms caused by seismic action, to which masonry structures are particularly vulnerable. In this regard, on-field observation carried out during post-earthquake damage assessments led to the classification of recurring damage patterns and the definition of analytical expressions, based on the application of the principle of virtual work and on newly upgraded formulation [3,4], able to estimate a collapse multiplier (load factor) for each recurring and codified damage mechanism [5,6].

Among the recurring collapse mechanisms, the overturning of the buildings' external walls (first damage mode or out-of-plane failure) represents the most severe condition of vulnerability in masonry buildings, and it is highly dependent on the lack of connection between perimeter and internal load bearing walls [7].

\* Corresponding author.

E-mail addresses: [antoniomurano1987@gmail.com](mailto:antoniomurano1987@gmail.com) (A. Murano), [A.A.Mehrotra@tudelft.nl](mailto:A.A.Mehrotra@tudelft.nl) (A. Mehrotra), [javier.ortega@csic.es](mailto:javier.ortega@csic.es) (J. Ortega), [hrodrigues@ua.pt](mailto:hrodrigues@ua.pt) (H. Rodrigues), [graca@civil.uminho.pt](mailto:graca@civil.uminho.pt) (G. Vasconcelos).

<https://doi.org/10.1016/j.engstruct.2023.116466>

Received 16 September 2022; Received in revised form 16 May 2023; Accepted 9 June 2023

0141-0296/© 2023 Elsevier Ltd. All rights reserved.

Therefore, starting from the contribution of historical essays describing the main characteristics of a traditional construction [8,9], further studies have been carried out aiming at correlating reference mechanical properties (e.g. Young's modulus, shear modulus, compressive strength, and shear strength) to a set of selected key-parameters (e.g. vertical joints configuration, horizontal joints configuration, etc.), resulting in the definition of the so-called Masonry Quality Index method (MQI) [10].

With regard to the structural analysis of masonry buildings, several modelling approaches, ranging from highly simplified to highly advanced, have been developed to numerically simulate the behaviour of masonry structures [11].

Each of these approaches has pros and cons in terms of accuracy and computational effort. Moreover, the derivation/estimation of input parameters (from empirical formulas or experimental data) has a great influence on the final output, affecting the reliability of the numerical simulations.

Even though the array of numerical strategies used for both academic purposes and professional practice is extremely wide, a categorisation of these procedures can be provided considering the level of refinement achieved once the numerical model is built [12,13,11].

In macro-modelling approaches (1), masonry can be modelled as one-phase material, where units, mortar and units-mortar interfaces are smeared out in a homogeneous continuum (Fig. 1a). Simplified micro-modelling approaches (2), on the other hand, rely on the definition of "expanded" masonry units combined with zero-thickness interface elements to simulate mortar joints behaviour (Fig. 1b). Conversely, in a detailed micro-modelling approach (3) masonry is represented as a three-phase material (Fig. 1c) implying that masonry units and mortar joints are represented by continuum elements whereas the unit-mortar interface is represented by discontinuous elements.

Macro-modelling has typically been the preferred approach for modelling complex historical masonry buildings (e.g. churches, towers, fortresses) [11,14–16] or complex structural systems such as building aggregates [17–19] because it represents a good compromise between results' reliability and computational effort, especially when the buildings to be analysed are considerably large. Indeed, the computational effort of FE macro-model analyses is considerably lower than comparable analyses conducted using detailed and simplified FE micro-modelling [20,21]. Moreover, in the literature, FE micro-modelling has mainly been applied to the structural analysis of constructions comprising single-leaf regular masonry walls [22–25]. These types of masonry constructions are easier to analyse using this approach due to the reduced complexity of the system in comparison with other masonry morphologies, e.g. three-leaf walls, or irregular ones.

Over the last two decades, the discrete element method (DEM) has become an effective alternative modelling approach for simulating the behaviour of masonry structural systems. DEM is particularly suited for detailed models used in research and interpretation of experimental results. Moreover this method allows to model block systems undergoing large motions and, from a computational standpoint, the use of explicit

time-stepping algorithms in DE codes results in a smaller run time per step if compared to codes based on implicit algorithm methods [26].

DEM early-stage applications to masonry structures involved the simulation of the behaviour of curved blocky structural systems [26], as well as the study of masonry constructions characterised by easily replicable and recurring geometrical patterns (e.g. obelisks, aqueducts, Greek temples) [27,28].

Many literature contributions also address the analysis of single-leaf masonry panels studied both under in-plane and out-plane loading conditions [29,30], while also investigating the influence of mechanical parameters on the overall structural performance of the selected case study [31–33].

Although some comparative studies addressing the performance of different modelling approaches in simulating the behaviour of masonry structures can be found in the literature [34,35], however, for both FE and DE-based modelling approaches, the body of knowledge related to the analysis of the out-of-plane failure mechanisms of two-leaf masonry walls, could be further expanded.

Several aspects, ranging from the interaction between the different leaves constituting the whole masonry panel to the study of the influence of mechanical properties and geometrical characteristics (e.g. masonry bond configuration), demand further attention due to their tendency to significantly influence on the seismic behaviour of masonry structures.

Despite the significant level of advanced numerical modelling techniques nowadays available to analyze the structural behavior of unreinforced masonry walls, the definition of standardized and sound rules accounting for the aforementioned epistemic uncertainties (geometrical and mechanical) is strongly needed [36].

Additionally, due to the high level of expertise required to properly define and calibrate refined models, the proposal of guidelines and recommendations to effectively support engineers and practitioners represent a significant open issue to be addressed [36].

This work presents a comparison among different numerical modelling strategies to simulate the out-of-plane behaviour of two-leaf stone masonry walls. The different strategies adopted are: (a) FE macro-model and a simplified micro-model approach by means of the FE software DIANA FEA [37]; and (b) simplified micro-modelling approach using the distinct element software 3DEC [38].

The experimental data adopted for the calibration of the models and the comparison of the results refers to an out-of-plane test carried out by means of an airbag on two different reduced scale (1:2) U-shaped stone masonry walls, namely an irregular dry-stone wall (DS) [39] and a masonry wall with regular stone units and mortar joints (REGW) [40].

Based on the aforementioned premises, the objectives of the paper are: (1) to present a systematic overview of the literature sources; (2) to provide a set of reference values and empirical formulation; (3) to define the main mechanical input parameters to characterize the mechanical behaviour of the models depending on the adopted modelling strategy; (4) to assess the reliability of different modelling approaches and commercial software packages in simulating the out-of-plane behaviour of

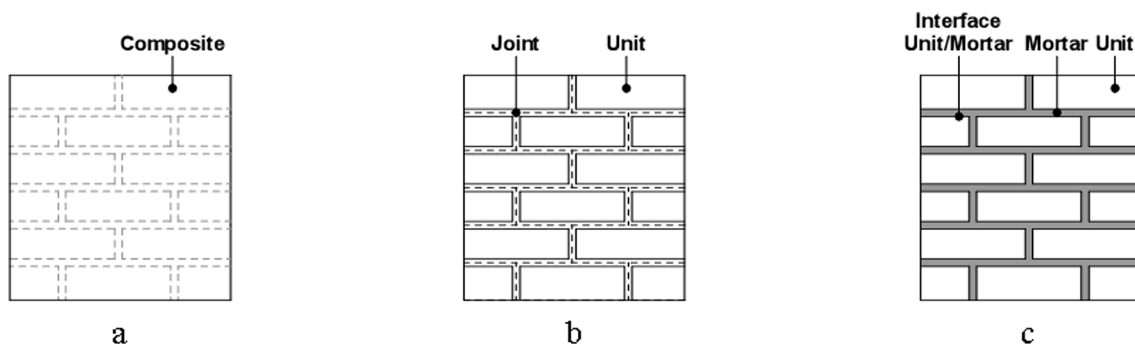


Fig. 1. Modelling strategies for masonry structures: (a) macro-modelling; (b) simplified micro-modelling; (c) detailed micro-modelling (adapted from [13]).

unreinforced masonry walls with complex geometry, namely two-leaf stone masonry walls with different bonds, since few studies in the literature analysed from a numerical standpoint these masonry typologies; (5) to highlight pros and cons of the selected modelling strategies accounting for results' accuracy and computational effort; (6) to provide insight to be used as a support/guidelines in practice-oriented engineering activities.

## 2. Description of the reduced scale masonry walls

The double-leaf stone masonry walls analysed in this work replicate the main characteristics of stone masonry walls commonly found in vernacular buildings in the northern region of Portugal [40], but similar morphologies can be found in other regions in Portugal, and other Mediterranean countries. In order to study experimentally their out-of-plane behaviour, reduced scale (1:2) masonry walls specimens with U-shaped plan configuration were adopted. The final wall specimens present a span of 2.25 m, a height of 1.35 m and a thickness of 0.30 m. In the experimental work two different types of masonry walls were considered, namely dry-stone wall (DS) [39] with roughly cut stone units and a regular stone masonry wall (REGW) [40] with mortared joints. In both specimens, through-stones (headers) were also used to ensure an adequate connection between the wall leaves; headers were distributed throughout the area of the walls, as shown in Fig. 2, where they have been highlighted in grey. Further details about the geometrical configuration of the reference stone masonry walls can be found in Martins [39] (drystone masonry wall) and Maccarini [40] (regular stone masonry wall with mortar joints).

Moreover, raw experimental data as well as CAD 3D models of both walls are available in an online repository (<https://doi.org/10.17632/pngbt7f4pv.1>).

The experimental setup was identical for both walls and the seismic action was simulated by means of an airbag (area of  $1.65 \times 1.35 \text{ m}^2$ ), exerting a uniformly distributed load on the rear surface of the wall's façade. Additionally, a vertical load was also applied to the transversal walls to simulate the self-weight of a timber roof. A supporting steel frame was placed between the reinforced concrete reaction wall of the laboratory and the airbag. Four load cells, placed between the steel profiles and the reaction wall, recorded the load applied by the airbag to the wall. The out-of-plane test was carried out under displacement control, with the control point located at the top of the frontal wall at mid-span, which is where the highest displacement was expected (Fig. 3).

The monitoring of the displacements of the frontal wall during the out-of-plane test was carried out using linear variable differential transducers (LVDTs), further details about the testing setup can be found in Martins [39], Maccarini [40] and Murano [41].

The force–displacement diagrams obtained from the out-of-plane tests of the drystone (DS) and regular stone masonry wall (REGW) are shown in Fig. 4a and Fig. 4b respectively. The force represents the sum of the forces recorded by the four load cells. The displacement is measured by the control LVDT (located at the top mid span of the wall).

Regarding the drystone wall (DS), the force–displacement diagram

highlights a relatively low resistance but a reasonable deformation capacity (approximately 70 mm). The wall shows increasing plastic deformations due to the small percentage of the deformation recovered during the unloading cycles of the test. This deformation pattern indicates that the displacement of the wall is caused by a progressively increasing sliding movement of the stones due to the absence of mortar joints able to limit this phenomenon.

This aspect can also explain the marked non-linearity in the pre-peak regime up to the maximum force (approximately 2.5 kN). Low levels of resistance are expected since the interlock between external and internal leaf is just provided by the presence of through-stones. Additionally, it is observed that the lack of connections in the corners affects the deformation of the wall, resulting in an asymmetric damage pattern.

Overall, the façade shows a cracking pattern governed by an out-of-plane movement. The opening of three vertical cracks was observed along the joints of the stones: (1) at the top mid-span of the wall along the through-stones (Fig. 5b–e); (2) at the intersection between façade and transversal walls (Fig. 5a–c–d–f). The most significant cracks arose in the left half of the wall (see convention adopted in Fig. 2). Small stone fragments filling the joints, and some stones from the outer surface ended up falling, creating voids in the wall in the final phase of the test. The effectiveness of the connection and of the interlock among stone units significantly affected the final damage pattern. In fact, on the right transverse wall the damage is barely visible, with only two small vertical cracks being observed, proving a better quality of the masonry bond (Fig. 5a–d).

The response of the regular wall (REGW) is characterized by a linear elastic regime approximately up to the peak load. The initial stiffness exhibits a reduction when approaching a load level around 40 kN. After the maximum resisting load of 47.8 kN the wall shows a notably higher deformation rate (Fig. 4). The post-peak behaviour is characterized by a relatively smooth softening branch corresponding to the decrease of the force for increasing lateral displacements. The test was stopped (due to safety reason) after reaching an out-of-plane displacement of approximately 40 mm.

The final cracking pattern of the regular wall (REGW) shows a diagonal crack in the external surface of the frontal wall arising from the mid-span at the top towards the left bottom corner (see convention adopted in Fig. 2), characteristic of the out-of-plane bending failure mode (Fig. 6b–e). In addition, a vertical crack also developed at the right transversal wall, adjacent to the connection to the frontal wall (Fig. 6a–d). At the back surface of the U-shaped wall, a significant horizontal crack developed in the frontal wall along the second bed joint from the bottom base, showing the formation of a clear overturning mechanism (Fig. 6d–f).

It should be noted that the crack at the left corner passes through the whole thickness of the wall, contrarily to the crack that developed at the right corner, which is only visible at the back surface. The development of this crack explains the lack of symmetry in the diagonal crack pattern at the front wall, also depending on the small irregularities in the construction process.

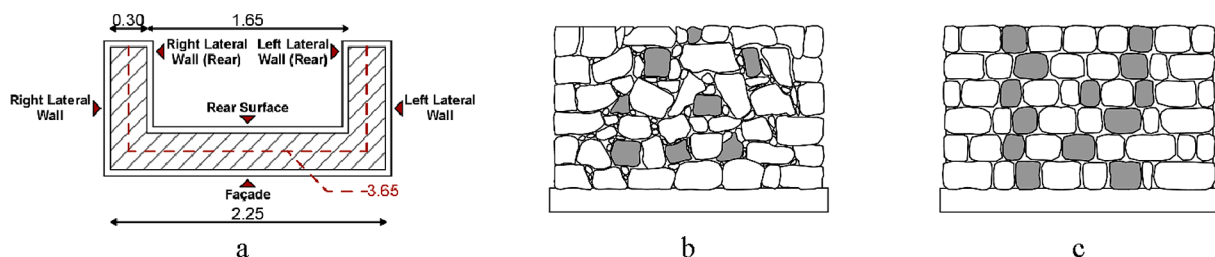


Fig. 2. Plan configuration tested specimens (a); front view drystone masonry wall (DS) [39]; (c) front view regular stone masonry wall (REGW) [40].

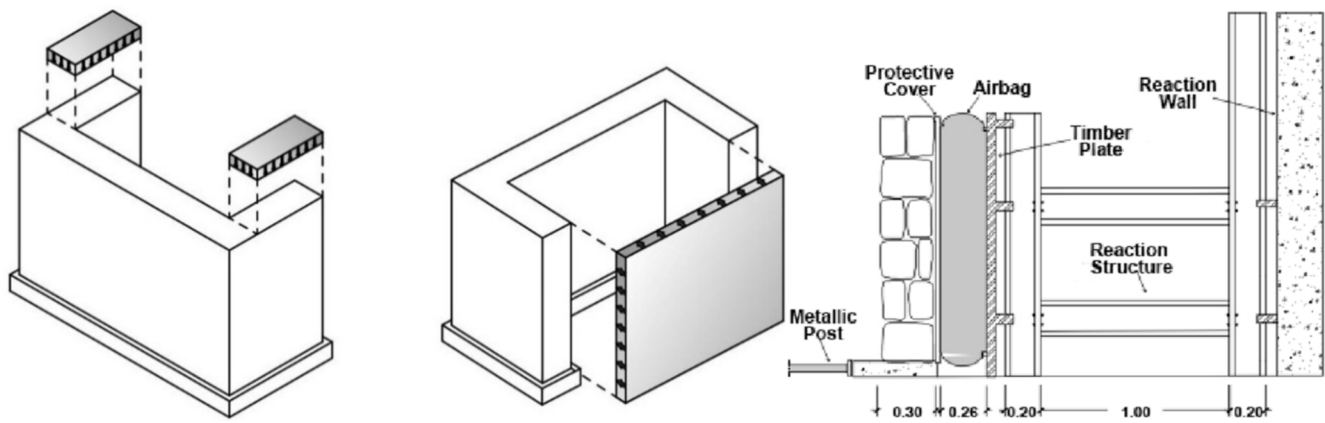


Fig. 3. Load configuration and test setup configuration adopted for the OOP test [39–41].

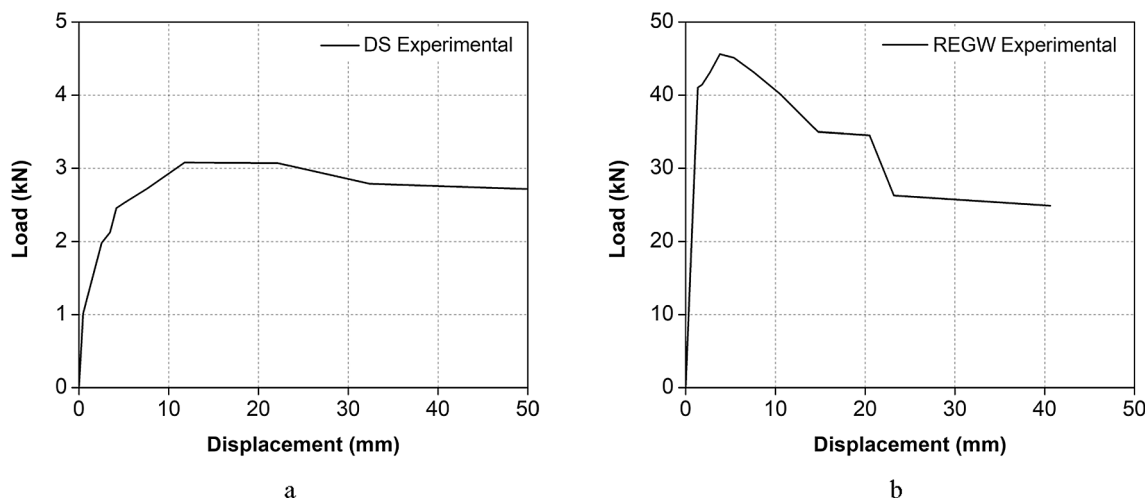


Fig. 4. Experimental force–displacement diagrams drystone wall (a) and regular stone masonry wall (b).

### 3. Finite elements macro and micro-modelling: Brief overview

Macro-modelling is an extremely effective approach due to its lower calculation demands. In practice-oriented analyses on large structural members or full structures, a detailed description of the interaction between units and mortar may not be necessary. Hence, macro-modelling approximates masonry as a homogeneous isotropic continuum material. The practical advantage of this approach relies on the use of simpler finite element (FE) meshes since there is no need of accurately simulating masonry components [13].

One of the most challenging tasks related to the use of macro-models is the formulation of adequate homogeneous constitutive laws able to simulate the mechanical features of masonry (e.g. anisotropy in the elastic regime, different compressive and tensile behaviour, post peak response). Constitutive laws for masonry could be described based on experimental results (direct approach) or deduced using homogenization techniques, which link the structural-scale model to a material-scale model of a representative volume element (RVE) of the structure [11]. Damages are described as a smeared property spreading over a large volume of the structure, which is an approximation that may lead to some inaccuracy because actual cracks in masonry structures usually arise in concentrated or isolated locations [42].

The detailed micro-modelling approach considers independently masonry units, mortar joints and mortar-unit interfaces. It is an extremely accurate method although it is highly time-consuming. Therefore, it is mainly applied to study limited portion of structures or

to analyse elastic and inelastic properties of units and mortar since their mutual interaction can be realistically described.

Simplified micro-models overcome the computational drawbacks of the standard micro-modelling technique. In this approach, a sort of “average interface” merges together each mortar joint and two adjacent unit-mortar interfaces, whereas the units are expanded to keep constant the overall geometrical configuration. Thus, expanded units represented by continuum elements are used to model both units and mortar material, whereas the behaviour of the mortar joints and unit-mortar interfaces is lumped to the discontinuous elements [43].

Macro and micro-models have been extensively used to analyse the seismic response of a wide range of masonry structures characterised by different boundary and load conditions [44–46]. Despite the limitations mentioned above, both approaches have proved their reliability in capturing the out-of-plane behaviour of masonry structures, showing a good agreement with the experimental results presented in research works available in the literature [20,47,48].

#### 3.1. Description of the finite elements macro-models

The numerical macro-model of the walls was defined with DIANA software using twenty-node tetrahedron solid 3D elements (CHX60). Each isoparametric solid element has 60 degrees of freedom and it is based on quadratic interpolation and Gauss integration [37]. Since the model is intended to simulate the experimental test, the concrete base was also included in the numerical model using the same solid 3D

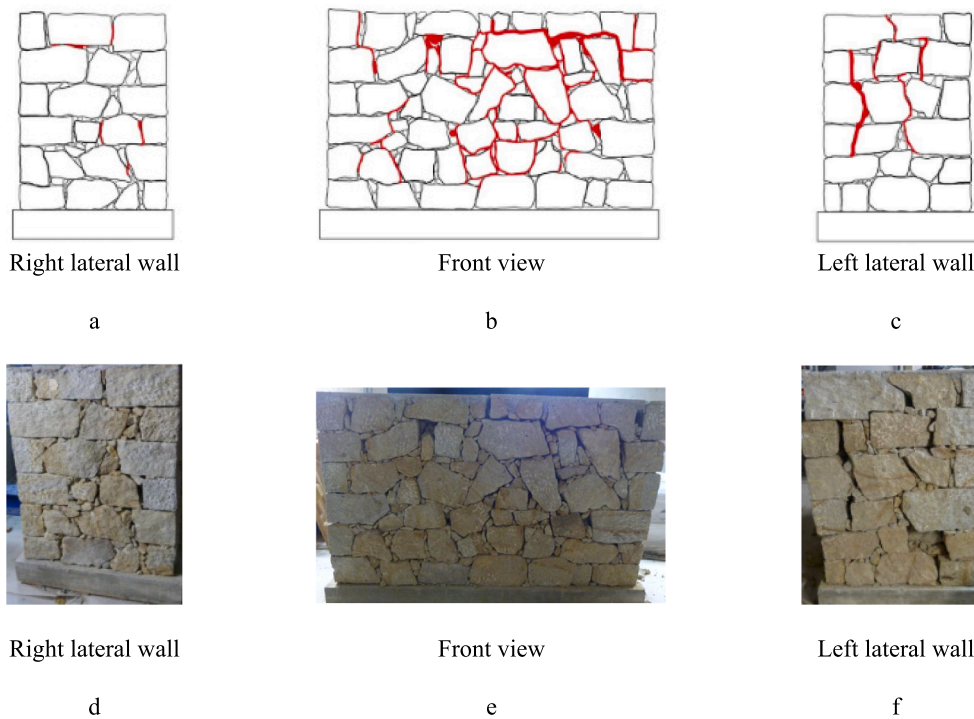


Fig. 5. Experimental damage pattern drystone wall (DS) [39].

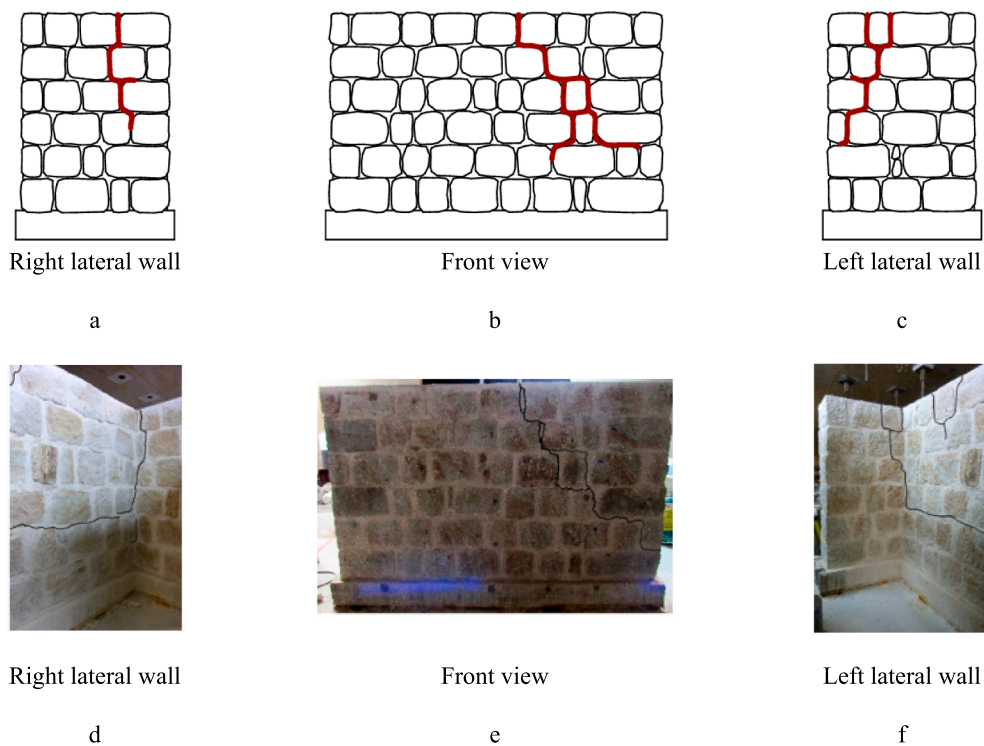


Fig. 6. Experimental damage pattern regular stone masonry wall (REGW) [40].

elements. Full connection was considered between the wall and the concrete base (translations and rotations fully constrained), assumed to exhibit a linear elastic behaviour.

The material model adopted to represent the non-linear behaviour of the stone masonry is a standard isotropic Total Strain Rotating Crack Model (TSRM). The model describes the tensile and compressive behaviour of the material with one stress-strain relationship and

assumes that the crack direction rotates with the principal strain axes [37]. An exponential softening function simulates the non-linear behaviour of the material in tension, whereas a parabolic function was adopted to describe the crushing behaviour in compression [37]. From a geometrical standpoint, both drystone (DS) and regular stone masonry wall (REGW) macro-models are exactly the same, whereas they differ for the mechanical properties assigned (see Fig. 7). The overall size of the

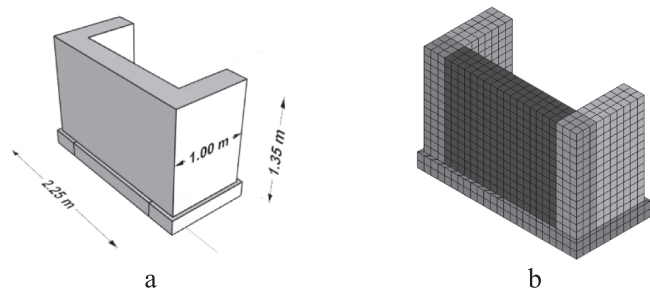


Fig. 7. Geometrical 3D model for finite element based macro-modelling application (a) and final macro model (b).

finite elements mesh is equal to 0.10 m.

The vertical loads acting on the model are the self-weight and a uniformly distributed load on each lateral wall equal to a resulting force of 10 kN (simulating the weight of structural elements such as the roof acting on the top of the structure).

The structural response of all the macro-models considered (both for the drystone and the regular wall) is described by a capacity pushover curve, which represent the horizontal load versus the displacement at the control point taken at the same position where the control LVDT was placed in the experimental test (top mid-span of the frontal wall).

The pushover analysis is based on the incremental application of a uniformly distributed horizontal load in the rear surface of the frontal wall (simulating the action exerted by the airbag); the analysis is considered completed when approaching the displacement level attained in the experimental test (assumed as a conventional state of collapse of the tested wall).

### 3.2. Description of the finite elements micro-models

The finite element based micro-model has been constructed starting from a 3D CAD file imported into DIANA software. To this end, it is important to point out that the overall geometry has been simplified and regularized by removing from the final 3D model all those stones with a reduced sized used to fill the joints of the wall. Once imported the geometric characterization of the model was concluded, the next task consisted in the application of interface elements connecting the stone units. A 3D interface available in DIANA for the connection of solid elements has been applied (CT361, 6 nodes triangular interface). Coulomb friction constitutive model has been assigned to the interface elements, implying that cracks occur at the masonry joints, whether they are dry or mortar joints [37].

Hence, the nonlinearities characterizing the mechanical behaviour of the wall are concentrated in the joints, whereas stone units (modelled using solid 3D elements, CHX60) are assumed to have linear elastic behaviour. The final geometrical and finite element models for both walls are presented in Fig. 8. In order to have a good representation of the strain and stress distribution, the average size of the finite elements mesh considered for the stone units and their interfaces is equal to 0.05 m.

The vertical loads acting on the model are the same considered for the finite element based macro-model (self-weight and a distributed load of 10 kN for each lateral wall). The base of the model is fully constrained and assumed to have a linear elastic behaviour. In order to define the structural response of the micro-models, a pushover analysis has been carried out following the same procedure applied for the macro-models (see Section 3.1).

### 4. Distinct element method (DEM): Brief overview

The “distinct element method” (DEM) was proposed by Cundall in 1971. Its theoretical assumptions are rooted in the field of rock

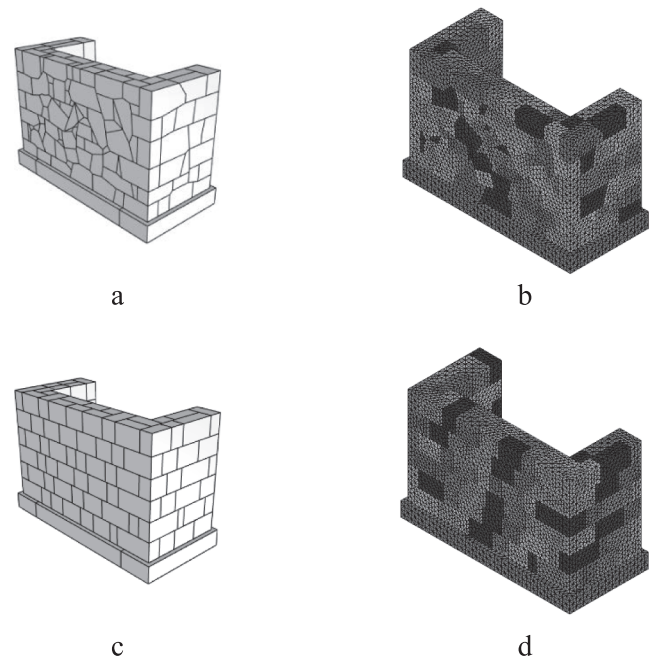


Fig. 8. Geometrical 3D model for simplified finite element based micro-modelling drystone masonry wall (a); Drystone masonry wall (DS) final finite element micro model (b); Geometrical 3D model for simplified finite element based micro-modelling regular stone masonry wall (c); Regular stone masonry wall (REGW) final finite element micro model (d).

mechanics and slope analysis, for which the conceptual model of a jointed rock mass as an assembly of rigid blocks was common in the 1960s.

In many DE models the interaction between blocks is represented by a set of contact points. Each contact force is a function of the relative block displacement at a specific point. In 2D models, a length is assigned to each contact point, whereas in three dimensions an area is assigned.

Thus, stresses are calculated according to the joint constitutive models typically formulated in terms of stresses and relative displacements. This approach makes it possible to handle different types of geometric interaction and large block movements [26].

The mechanical behaviour of contacts in DE models can be represented using two models: 1) the hard contact model, which envisages the condition of no overlap between blocks and 2) the soft contact model, in which contact stiffness is defined in the normal and shear directions and a small overlap occurs when the contact is in compression; the latter hypothesis is usually preferred in most DE formulations.

In the shear direction, Coulomb friction is the most widely accepted model for masonry joints. Hence, in DE codes that assume deformable contacts and the point contact approach, the normal contact force ( $\Delta F_n$ ) and shear contact force ( $\Delta F_s$ ) increments are calculated from the increments of relative displacement between blocks in the normal direction ( $\Delta u_n$ ) and shear directions ( $\Delta u_s$ ) as [26]:

$$\Delta F_s = k_s A_c \Delta u_s \quad (1)$$

$$\Delta F_n = k_n A_c \Delta u_n \quad (2)$$

where the  $k_n$  and  $k_s$  are the normal joint stiffness and shear joint stiffness and  $A_c$  denotes the contact area.

From a mechanical standpoint, blocks are assumed to have a rigid behaviour. This option (present in all DE codes) is highly suitable for all those practical problems in which failure via specific collapse mechanisms is common (e.g. assessment of the collapse loads in stone masonry construction). For such problems, the structural deformation can be concentrated in the elastic contacts (deformable contact models) or



assumed to be negligible (hard contact models).

The basic assumptions related to a computer-based discrete element modelling approach are [26]: (1) development of finite displacements and rotations of discrete bodies (blocks), including the complete detachment; (2) automatic recognition of new contacts between blocks as the calculation progresses.

#### 4.1. Distinct element method (DEM): 3DEC software

In 3DEC, the software developed by Itasca that is used in this work [38], masonry is represented as an assemblage of discrete blocks (rigid or deformable) connected by zero thickness interfaces representing mortar joints. Deformable blocks are internally discretised into a finite number of constant strain tetrahedral elements. Nonetheless, as opposed to FEM, in DEM, a compatible finite element mesh between the blocks and the joints is not required [29].

Rigid blocks are suitable to simulate the behaviour of a structural system that is governed by the joints characteristics. Blocks are connected to each other by a sets of point contacts, located at the outer perimeter of the blocks themselves. For each contact point, there are two spring connections (Fig. 9), transferring either a normal force or a shear force from one block to another [26,29].

A zero-thickness interface between adjacent blocks simulates the joints behaviour by means of a Mohr-Coulomb model with a tension cut-off, which considers both shear and tensile failure (Fig. 10).

In the elastic range, the incremental normal and shear stresses on a joint are computed by multiplying normal and shear displacements by normal ( $k_n$ ) and shear stiffness ( $k_s$ ) [38]:

$$\Delta\sigma_s = k_s \Delta u_s \quad (3)$$

$$\Delta\sigma_n = k_n \Delta u_n \quad (4)$$

where  $\Delta\sigma_n$  and  $\Delta\sigma_s$  are the incremental normal and shear stress respectively, whereas  $u_n$  is the normal displacement and  $u_s$  is the shear displacement. The maximum shear stress allowed is given by [38]:

$$\sigma_F^{peak} = c + \sigma_{n,max} \bullet \tan\phi \quad (5)$$

where  $c$  is the cohesion,  $\sigma_n$  is the normal stress and  $\phi$  is the friction angle. After the peak strength has been reached, shear strength drops until a residual strength stress calculated as (Fig. 3 - a):

$$\sigma_F^{res} = c_{res} + \sigma_n \bullet \tan\phi_{res} \quad (6)$$

where  $c_{res}$  is the residual cohesion, and  $\phi_{res}$  is the residual friction angle.

After the shear strength has been exceeded, it is possible for the zero-thickness interfaces to dilate with continued shearing (e.g. mortar fails in shear), see Fig. 10b. The normal displacement, corresponding to the opening of the joint in the normal direction during shear loading, can be expressed as [38]:

$$\Delta u_{n,dil} = \Delta u_s \bullet \tan\psi \quad (7)$$

where  $\psi$  is the dilatancy angle and  $\Delta u_n$  is the normal displacement. The equation for normal stress can be adjusted considering the effect of dilation as follows:

$$\sigma_{n,tot} = \sigma_{n,elast} + \sigma_{n,dil} = k_n \Delta u_n + k_n \Delta u_{n,dil} = k_n \Delta u_n + k_n \bullet \Delta u_s \tan\psi \quad (8)$$

When dilation is present, the shear displacement is in the plastic phase ( $\Delta u_s > \Delta u_{s,elast}$ ), see Fig. 10a. The normal displacement is assumed to be linear until  $z_{dil}$  (Fig. 10b). Dilation increases if the increment of shear displacement runs in the same direction as the total shear displacement. The extension occurs until the limiting shear displacement ( $z_{dil}$ ) is reached. Under axial loads, elastic behaviour is assumed in the interfaces until tensile failure occurs (Fig. 10c).

Mechanical damping is used in the distinct element method to solve two general classes of problems, namely static (non-inertial) and dynamic solutions. The damping models available in 3DEC are: (1) adaptive global damping and (2) local damping [38]. Itasca's 3DEC manual recommends the use of local damping for static analyses since it allows to minimise oscillations that may arise when abrupt failure occurs in the model.

Over the past two decades, 3DEC has proved to be quite versatile in modelling the behaviour of different types of structural systems, such as masonry wall panels [29,30], reduced scale mock-ups of masonry structures [49], historical stone masonry structures with irregular masonry bond geometrical configuration [50], stone masonry arches and aqueducts [51–53] and column-architrave structures under seismic action [54,55,28].

#### 4.2. Description of the distinct elements micro-models

The simplified micro-models built using 3DEC software envisages the use of rigid blocks (undeformable) to simulate masonry stone units both in drystone wall (DS) and in regular stone masonry wall (REGW), whereas the nonlinear behaviour is simulated by means of interface contact points based on a Mohr-Coulomb constitutive model, which have been used to simulate the joints behaviour in both models (DS and REGW) [38]. Fig. 11 presents the final geometrical and distinct element models for both walls. Despite the 3D models imported in 3DEC software are the same used in DIANA, the definition of the contact interfaces among stone units has been significantly faster. Stone units are assumed to have a linear elastic behaviour, as well as the concrete base of the wall that is fully constrained.

The input parameters required to characterize the mechanical behaviour of the interface are normal/shear stiffness, cohesion, tensile strength, dilatancy and friction angle. Dilatancy has been assumed equal to zero in both models (DS and REGW). Damping models and default values suggested in 3DEC manual have been considered [38]. Cohesion and tensile strength have been assumed equal to zero to simulate the same physical configuration of the drystone wall. Conversely, in the regular stone masonry wall (REGW), the presence of mortar joints required a calibration of these values, which has been carried out starting from values collected from sources available in the literature. Average values proposed in the literature have been also considered for



Fig. 9. Contact between two blocks [38].

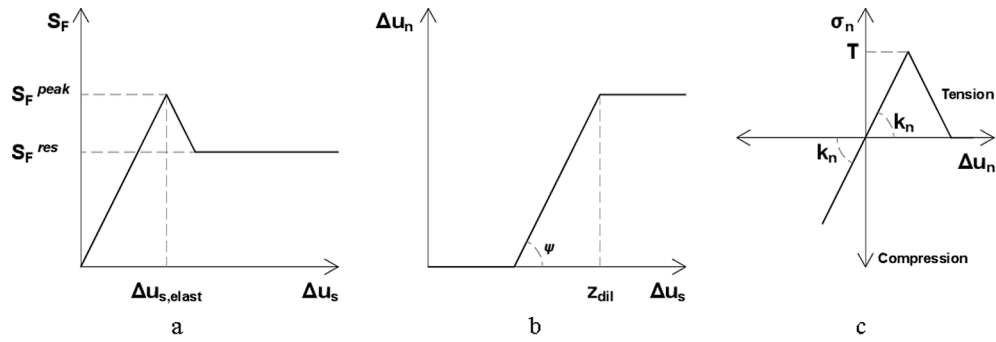


Fig. 10. Mechanical behaviour of interfaces: (a) Mohr-Coulomb slip model; (b) bilinear dilatant model; (c) behaviour under uniaxial loading [29].

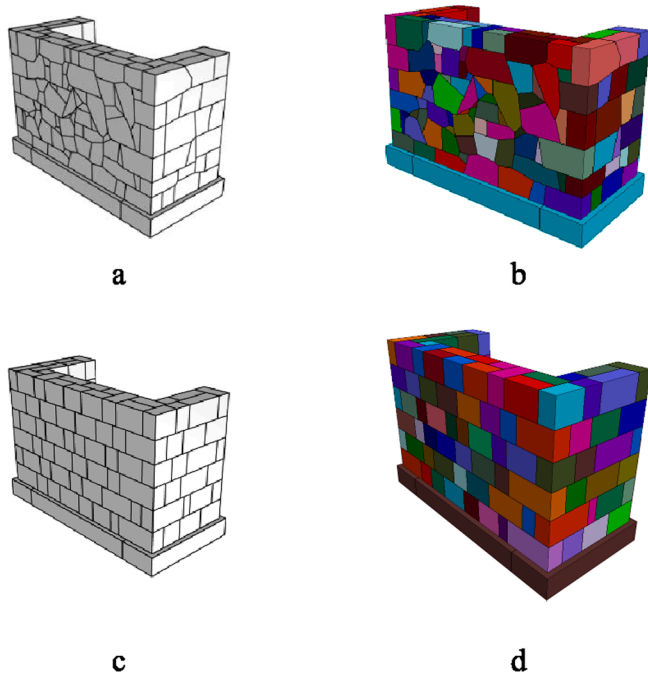


Fig. 11. Geometrical 3D model for simplified finite element based micro-modelling drystone masonry wall (a); Drystone masonry wall (DS) final distinct element micro model (b); Geometrical 3D model for simplified distinct element based micro-modelling regular stone masonry wall (c); Regular stone masonry wall (REGW) final distinct element micro model (d).

friction angle and stiffness properties. Further details about parameters estimation and calibration procedures of both walls are presented in Section 5 and 6 respectively.

The vertical loads acting on both drystone and regular wall models are the self-weight and the distributed load of 10 kN acting on each lateral wall. The structural response of the model has been evaluate by means of pushover analyses (following the same criteria) as mentioned in Section 3.1 and Section 3.2 regarding the finite element based macro and micro models.

### 5. Estimation of mechanical properties in FE and DE models

As aforementioned, the modelling approaches considered in this study are: (1) macro-modelling and (2) simplified micro-modelling. The macro-modelling analyses will be carried out using a FE-based commercial software (DIANA [37]), whereas for the simplified micro-modelling, two different software, namely DIANA [37] and the DEM-based software 3DEC by Itasca [38], will be used.

The main challenges regarding the development of a numerical model are, on one hand, the definition of a geometrical model that

Table 1

Summary of the main parameters needed for macro-modelling and simplified micro-modelling (adapted from [56]).

	Elements	Linear parameters	Nonlinear parameters
Macro-modelling	Homogeneous continuum (units and joints): Isotropic	Young's Modulus Poisson ratio Density	Tensile and Compressive strength Fracture Energy in tension and in compression
Simplified Micro-modelling	Expanded units: assumed isotropic	Normal and Shear Stiffness	None (All the nonlinearities are lumped at the interfaces, i.e., Masonry joints and potential cracks in the units)
	Joints (bed and head): Interface elements	Normal and Shear Stiffness	Bond tensile strength; Cohesion; Friction Angle; Dilatancy; Mode I and Mode II fracture energy

accurately replicates the reference structure without being excessively detailed and, on the other hand, the effective estimation of the mechanical properties that characterise the materials' behaviour.

To that end, as highlighted in Section 2, macro-modelling approaches consider masonry as an isotropic continuum material having linear and non-linear properties. Conversely, in a simplified micro-model it is assumed that the non-linear properties of masonry are concentrated on the interface connecting the units (see Table 1). Hence, the input parameters required to carry out the numerical analysis may vary according to the modelling approach adopted and the software characteristics, with the latter factor depending also on the constitutive model selected to simulate the behaviour of a certain structural system.

The estimation of the mechanical properties related to the macro-modelling approach is typically based on the recommendations provided by Lourenço [13], consisting of a set of empirical expressions which link the macro-model's mechanical properties to a reference parameter, namely the Young's Modulus of masonry, usually determined by means of experimental testing procedures. The equations used to estimate macro-model mechanical properties in this study are:

$$f_c = \frac{E}{\alpha} \quad (9)$$

$$f_t = \frac{1}{10} f_c \quad (10)$$

$$G_{fc} = d_{u,c} \bullet f_c \quad (11)$$

$$G_{f1} = 12N/m \quad (12)$$

Where  $E$  is the Young's Modulus,  $f_c$  is the compressive strength,  $\alpha$  is a coefficient assumed to be equal to 1000,  $f_t$  is the tensile strength,  $G_{fc}$  is the compressive fracture energy,  $d_{u,c}$  is the ductility index in compression assumed equal to 1.60 mm and  $G_{f1}$  is the Mode I fracture energy

[13]. It must be noted that the values of  $\alpha$ ,  $d_{u,c}$  and  $G_{f1}$  have been set based on the same set of recommendations, as already proposed in other works concerning the macro-modelling of masonry structures [57,47].

An important aspect related to the comparison of the modelling strategies presented in this study involves the use of suitable equations enabling the transition from one modelling approach to another depending on the input data available (e.g. estimation of Young's Modulus starting from joints' normal stiffness and vice versa). In fact, the calculation of interface stiffness is a crucial aspect for the application of simplified micro-modelling approaches both for FE-based software and for DE-based software. Therefore, providing reference values for interface elements can represent a good starting point in the calibration procedure characterising any numerical simulation, especially when initial information is limited and/or few experimental data is available.

According to Itasca manual [38], the relation between Young's Modulus and normal and shear stiffness can be expressed as:

$$\frac{1}{E_m} = \frac{1}{E_{m,u}} + \frac{1}{k_n \bullet s} \quad (13)$$

$$k_n = \frac{E_m \bullet E_{m,u}}{s \bullet (E_{m,u} - E_m)} \quad (14)$$

$$k_s = \frac{k_n}{2 \bullet (1 + \nu)} \quad (15)$$

Since 3DEC's initial field of application was geotechnical engineering, these equations originally referred to uniaxial loading of rock containing a single set of uniformly spaced joints oriented normal to the direction of loading. The equations have been adjusted in order to be applied to masonry structures, hence  $E_m$  is the masonry equivalent modulus (formerly rock mass Young's modulus);  $E_{m,u}$  is the block Young's Modulus (formerly intact rock mass Young's modulus),  $k_n$  is the joint normal stiffness,  $k_s$  is the joint shear stiffness,  $s$  is the thickness of the mortar joints (formerly joint spacing), which for the purpose of this study is assumed equal to 1 cm.

Sarhosis and Sheng [32] investigated the parameter prediction problem for masonry constitutive micro-models, proposing a methodology based on an optimization technique to minimise the differences between results obtained experimentally and computationally. Once bricks and mortar properties are known, the first estimation of normal and shear stiffness is obtained using the following equations:

$$Jk_n = \frac{E_b \bullet E_m}{h_m \bullet (E_b - E_m)} \quad (16)$$

$$Jk_s = \frac{G_b \bullet G_m}{h_m \bullet (E_b - E_m)} \quad (17)$$

$$G = \frac{E}{2 \bullet (1 + \nu)} \quad (18)$$

Where  $E_b$  is the blocks Young's Modulus;  $E_m$  is the mortar Young's Modulus;  $G_b$  is the blocks Shear Modulus (estimated using equation (16));  $G_m$  is the mortar Shear Modulus (estimated using equation (16));  $h_m$  is the thickness of the mortar joints;  $\nu$  is the Poisson ratio = 0.2 (assumed value);  $Jk_n$  is the joint normal stiffness;  $Jk_s$  is the joint shear stiffness.

Other relations to predict the normal and shear stiffness of masonry joints were provided by Bui et al [29], who studied in-plane and out-of-plane behaviour of masonry walls by comparing numerical simulations and experimental results. Masonry panels or masonry mock-ups were made with brick (simulated by means of rigid elements) and dry joints (simulated by means of zero-thickness interface elements). The elastic stiffness properties for interface elements have been obtained using the following equations:

$$k_n = \frac{E_b \bullet E_m}{h_b \bullet (E_b - E_m)} \quad (19)$$

$$k_s = \frac{k_n}{2 \bullet (1 + \nu)} \quad (20)$$

Where  $E_m$  is the masonry equivalent modulus assumed;  $E_b$  is the block Young's Modulus;  $k_n$  is the joint normal stiffness;  $k_s$  is the joint shear stiffness;  $h_b$  is the height of the masonry unit.

Similarly, Gonen et al analysed the seismic capacity of a stone masonry Roman aqueduct (Valens Aqueduct), constructed in the 4th century CE in Istanbul (Turkey), using the discrete element method (DEM) [53]. The modelling approach comprises distinct rigid blocks interacting along their boundaries based on the point-contact hypothesis. The normal stiffness ( $k_n$ ) was predicted based on the ratio between masonry elastic modulus ( $E$ ) and horizontal joint spacing ( $h$ ), which includes one brick plus the mortar joint thickness (Equation (21)). The shear stiffness ( $k_s$ ) was calculated through the theory of elasticity (Equation (22)):

$$k_n = \frac{E}{h} \quad (21)$$

$$k_s = \frac{k_n}{2 \bullet (1 + \nu)} \quad (22)$$

In addition to the expressions previously presented, data collected referring to interface properties in masonry structural systems (e.g. complex buildings, laboratory mock-ups, ancient aqueducts, column-architrave classical structures) with dry joints and mortar joints, is presented in Table 2 and Table 3 respectively. Besides normal stiffness ( $k_n$ ) and shear stiffness ( $k_s$ ), information is also included regarding joint tensile strength ( $f_t$ ), cohesion ( $c$ ) and friction angle ( $\phi$ ). It must be noted that, in all the works examined, the dilatancy ( $dI$ ) value is assumed to be zero.

The values related to the mechanical properties reported in Table 2 and Table 3 resulted from specific experimental campaigns (e.g. dynamic identification tests) or reference values provided in the literature.

However, it must be noted that in all the consulted documents, the initial mechanical properties, whether they were defined using experimental data or mathematical expressions, required further adjustments to fit the experimental data (if available) and/or to define a DE model able to accurately replicate the actual behaviour of the analysed structural system.

Overall, based on the information gathered, in both drystone masonry and masonry with mortar joints, the ratio between normal and shear stiffness ranges from 2 to 2.4 ( $k_n = 2-2.4 k_s$ ) and the cohesion to tensile strength ratio ranges from 1.25 and 1.5 ( $c = 1.25 - 1.50 f_t$ ). The friction angle values range from 30° to 40° and from 30° to 45° for drystone masonry and masonry with mortar joints respectively.

In the present study, the normal stiffness was assumed as  $k_n = 2k_s$  and the cohesion was estimated as 1.25  $f_t$ , following a more conservative estimation since no experimental data regarding the mechanical characterization of stone and mortar was available. Any variation characterising the calibration procedure has been carried out keeping these ratios constant. To conclude, Table 2 and Table 3 presents also the average values related to the joints' mechanical properties for dry stone masonry walls and mortared masonry walls respectively. The average parameters will be used as a starting point for the calibration procedure addressed in Section 6.

## 6. Calibration of numerical models and results

The calibration procedure, applied for both walls (DS and REGW), consists of the following steps: (1) preliminary analysis carried out using the simplified micro-model built with 3DEC software (DE-based software) since it allows to obtain an initial estimation of the model's structural behaviours with a smaller computation effort compared to the others modelling approach considered in this study, namely FE macro-modelling and FE-based micro-modelling. The starting mechanical properties used to characterise the behaviour of the interface elements

**Table 2**  
Summary of interface properties for drystone masonry.

Reference	Normal Stiffness - $k_n$ (N/m <sup>3</sup> )	Shear Stiffness - $k_s$ (N/m <sup>3</sup> )	Tensile Strength - $f_t$ (N/m <sup>2</sup> )	Cohesion - $c$ (N/m <sup>2</sup> )	Friction Angle - $\phi$ (°)
Sincraian et al., 1999 [58]	1.00E+11	1.00E+11	2.00E+6	0–7.00E+6	40
Drei et al., 2001 [59]	0	1.00E+11	0	0–5.00E+5	25–30
Mirabella et al., 2001 [60]	5.00E+10	2.00E+10	NA	0	30
Papantonopoulos et al., 2002 [54]	1–2.00E+9	1.00E+9	0	0	35–37
Psycharis et al., 2003 [55]	1.00E+9	1.00E+9	0	0	37
Psycharis et al., 2009 [27]	1.00E+9	1.00E+9	0	0	43–66
Oliveira et al., 2012 [61]	3.49E+9	1.75E+9	2.00E+6	0	35
Rouxinol et al., 2014 [62]	1.00E+9	4.00E+8	0	0	36
Lemos et al., 2015 [63]	4.00E+9	2.00E+9	NA	0	25–40
Sarhosis et al., 2016 [28]	4.00E+12	2.00E+12	0	0	14–36.80
Bui et al., 2017 [29]	1.96E+9	8.20E+08	NA	0	38
Bui et al., 2017 [29]	5.87E+9	2.45E+9	NA	0	35.50
Bui et al., 2017 [29]	8.08E+9	3.37E+9	NA	0	35.50
Bui et al., 2017 [29]	1.14E+11	4.73E+9	NA	0	35.50
Bui et al., 2017 [29]	1.30E+11	5.43E+9	NA	0	35.50
Bui et al., 2017 [29]	5.87E+9	2.45E+9	NA	0	30.40
Moranova et al., 2017 [52]	3.53E+9	1.48E+9	NA	0	25–35
Mordanova et al., 2017 [52]	2.90E+9	1.23E+9	NA	0	26–35
Pulatsu et al., 2018 [64]	4.39E+10	1.83E+10	2.67E+4	4.00E+4	35
Pulatsu et al., 2020 [65]	5.00E+9	2.50E+9	0	0	35
Average	2.43E+11	1.13E+11	4.03E+5	2.22E3	34.74

have been set equal to the average values proposed in Table 2 and Table 3, resulting from the literature review previously presented in Section 5; (2) the second step involves the adjustment of the preliminary numerical load–displacement pushover curve to fit the experimental results. The fitting process consisted in different pushover analyses (trial/error approach) carried out modifying the mechanical inputs of the model in terms of stiffness (keeping the ratio  $k_n = 2k_s$  as mentioned in Section 5) and maximum load capacity (keeping the ratio  $c = 1.25 f_t$ , as mentioned in Section 5). In REGW, friction angle value has been kept constant and assumed as the average of the values proposed in the literature for this specific masonry typology (see Table 3), whereas in the drystone masonry wall, the friction angle was reduced since the average value computed based on the sources gathered in the literature, resulted slightly higher for this specific masonry typology; (3) the normal stiffness value ( $k_n$ ) obtained at the end of the tuning process carried out in the previous step is used to: (i) estimate a corresponding value of Young's Modulus in order to define the corresponding properties to be used in the macro-model (see equations (9)–(11)); and (ii) to provide a first estimation of the shear stiffness ( $k_s$ ), based on the ratio  $k_n = 2k_s$ , presented in Section 5; (4) once the macro-model's mechanical properties have been defined, a modal analysis was carried out to compare numerical mode shapes and natural frequencies of vibration for all the considered modelling approaches (FE macro and micro-models, DE-based micro-model), to have a first insight regarding the effectiveness of the parameters' estimation procedure and the consistency of the behaviour of the models. An overview of the workflow is shown in Fig. 12.

### 6.1. Drystone wall (DS)

The load-displacements curves of dry stone wall obtained in the early stage of the calibration procedure (DS\_Micro\_DEM\_Step 1) and after the iterative fitting process carried out in order to match numerical and experimental data (DS\_Micro\_DEM\_Step 2) are presented in Fig. 13a and 13b respectively.

The first trial analysis (DS\_Micro\_DEM\_Step 1) carried out with a DE simplified micro-model shows a considerable overestimation both in terms of initial stiffness and in terms of peak value attained. Looking at the graph in Fig. 13a, it is possible to highlight a significant rigid behaviour of the model until reaching a load level of approximately 60 kN. Subsequently, the numerical curve displays a progressively increasing load level up to 80 kN, which lead to the out-of-plane failure of the wall. Once exceeded this threshold (80 kN), the curve is

characterised by a plateau-like trend displaying slightly increasing load levels corresponding to a progressively increasing displacement level.

Conversely, Fig. 13b displays a better consistency between numerical and experimental outcomes. Initially, numerical and experimental curves show a similar behaviour at least up to the load level of 1 kN. After that, the experimental curve shows more accentuated non-linear behaviour and a gradual loss of stiffness up to approximately 3 kN, which corresponds to the appearance of severe damage at the wall. The experimental plateau is characterised by slightly decreasing loading levels corresponding to increasing displacements levels. Regarding this latter aspect, DS\_Micro\_DEM\_Step 2 curve displays a gradually increasing trend both for load and displacement levels. On the other hand, the behaviour of the wall until the development of significant damage levels appears to be satisfactorily captured.

As previously stated for the drystone masonry wall, the first analysis has been carried out using the reference average values presented in Table 2, whereas the final input parameters are reported in Table 4. The significant inconsistency between the experimental outcome and the numerical curve DS\_Micro\_DEM\_Step 1, could be partly explained considering the heterogeneity of the data collected regarding drystone structural systems. The stiffness parameters used in the first trial analysis are, in fact, 66 times and 78 times higher than the final values adopted for normal and shear stiffness respectively. Additionally, in the second trial carried out using adjusted parameters, tensile strength and cohesion values have been set equal to zero to better match the experimental and numerical outcomes.

The final parameters characterising the interface properties are presented in Table 4; it must be noted that the values in brackets refer to the input parameters used in the first trial of the calibration procedure reported in Table 2.

Once the final mechanical properties for the DE-based simplified micro-model have been adjusted, the following step involved the estimation of a Young's Modulus to be used for the calculation of the remaining input parameters needed for the macro-model developed for the drystone wall.

To this end, starting from the value of normal stiffness  $k_n$  presented in Table 4, a first estimation of the Young's Modulus has been carried out based on the expressions provided in the literature (see Section 4, equations (14), (16), (19) and (21)). The main assumptions adopted to estimate an equivalent Young's Modulus of masonry for the drystone wall were: (1) the average height of stone units has been set equal to 0, 20 m (20 cm); (2) if requested by a specific equation, mortar Young's Modulus and joints' thickness have been considered extremely low

**Table 3**  
Summary of interface properties for masonry with mortar joints.

Reference	Normal Stiffness - $k_n$ (N/m <sup>3</sup> )	Shear Stiffness - $k_s$ (N/m <sup>3</sup> )	Tensile Strength - $f_t$ (N/m <sup>2</sup> )	Cohesion - $c$ (N/m <sup>2</sup> )	Friction Angle - $\mu$ (°)
Oliveira et al., 2002 [66]	1.00E+9	4.00E+8	0	5.00E+5	35
Oliveira et al., 2002 [66]	1.00E+9	4.00E+8	0	0	45
Oliveira et al., 2002 [66]	1.00E+9	4.00E+8	0	7.50E+5	30
Oliveira et al., [66]	1.00E+9	4.00E+8	0	7.50E+5	30
Schlegel et al., 2004 [67]	7.64E+11	2.47E+11	4.00E+5	5.00E+5	30 – 39
Alexandris et al., 2004 [68]	3.00E+10	3.00E+10	1.25E+5	1.00E+6	30
Alexandris et al., 2004 [68]	3.00E+10	3.00E+10	1.25E+5	1.00E+6	30
De Felice et al., 2005 [68]	3.00E+10	3.00E+10	1.25E+5	1.00E+6	30
De Felice et al., 2005 [69]	1.88E+9	7.53E+9	0	0	30
Sarhosis et al., 2014 [70]	7.64E+9	1.79E+9	1.00E+5	1.00E+5	35
Lemos et al., 2017 [49]	3.00E+9	1.50E+9	1.60E+5	3.20E+5	35
Gonen et al., 2021 [53]	1.67E+13	7.20E+12	1.00E+5	2.50E+5	35
Gonen et al., 2021 [53]	1.00E+13	4.20E+12	2.50E+5	1.25E+5	35
Average	2.00E+12	9.00E+11	1.07E+5	4.80E+5	32.73

(values close to zero), since no mortar joints are present in the drystone wall examined.

The results obtained using the different formulations are summarised in Table 5. The average value for the Young's Modulus of the drystone wall stands at  $3.98 \text{ E}+8 \text{ N/m}^2$  (400 MPa). It must be noted that, due to the characteristics of the formulation proposed by Sarhosis [32] which considers Young's Modulus for both stone units and mortar, it has not

been possible to estimate a value of equivalent Young's Modulus suitable for the purpose of this study.

Overall, the application of the inverse formulations yielded similar results confirming the consistency of the expression adopted, regardless of the initial assumptions applied to comply with the characteristics of the structural system analysed (drystone masonry wall).

Macro-model parameters related to the initial stage of the calibration procedure (DS\_Macro\_FEM\_Step 1) have been estimated starting a Young's Modulus value of 398 MPa ( $3.98\text{E}+8 \text{ N/m}^2$ ), resulted from the average of the results presented in Table 5.

According to the empirical equation proposed in Section 5, macro-model properties have been estimated and used as input parameters (see Table 6) to run a preliminary modal analysis and pushover analysis later compared to the results obtained by means of DE method. The initial results showed a significant overestimation of the Load-Displacement macro-model curve if compared to both numerical results (3DEC software simplified micro-modelling) and experimental results (Fig. 14).

As mentioned above, DS\_Macro\_FEM\_Step 1 curve has been obtained using the parameters reported in Table 6 (see column Step 1), resulted from the application of equations (9)–(12) reported in Section 5. It must be noted that these equations provide an estimation of compressive strength, tensile strength and compressive fracture energy based on the value of the Young's Modulus. Therefore, these parameters are linked to each other, except for the Mode I fracture energy which is set equal to 12 N/m as suggested in the literature [13].

Looking at Fig. 14, it is clearly visible a significant inconsistency of the macro-model curve (DS\_Macro\_FEM\_Step 1) if compared to experimental and numerical results obtained by means of DEM (DS\_Micro-DEM\_Step 2). The initial behaviour of the drystone wall analysed by means of the macro-model approach shows a considerably higher initial stiffness. The peak load is slightly higher than 20 kN, which is around 7 times higher than the corresponding peak loads (approximately 3 kN) detected both in the experimental curve and DE pushover analysis (curve DS\_Micro\_DEM\_Step 2).

The comparison between frequencies of vibration and mode shapes obtained from modal analysis carried out with macro and micro-modelling approaches also revealed an overestimation of natural frequencies of vibration in the macro-model (DIANA) with respect to the simplified micro-modelling approach in 3DEC (around 20 % higher for the first 2 modes of vibration and 3 % for the third one). On the other hand, no differences were detected in the mode shapes (Fig. 15). In addition, it should be stressed that no experimental data was available regarding the dynamic identification of the drystone masonry wall, hence, the results presented refer only to numerical simulations.

Taking into account the outcomes of the analyses regarding the parameters estimation in Step 1 of the calibration process, further adjustments on the mechanical properties related to the macro-model approach have been carried out to reach an acceptable consistency of the results (see Table 6, column Step 2).

In the DE analyses, the zero cohesion and zero tension assumptions result in a significant decrease in terms of stiffness and peak load as soon as the contact between two stone units weakens. This physical condition cannot be replicated in the macro-model because from a geometrical point of view, the model itself assumes a continuous configuration,

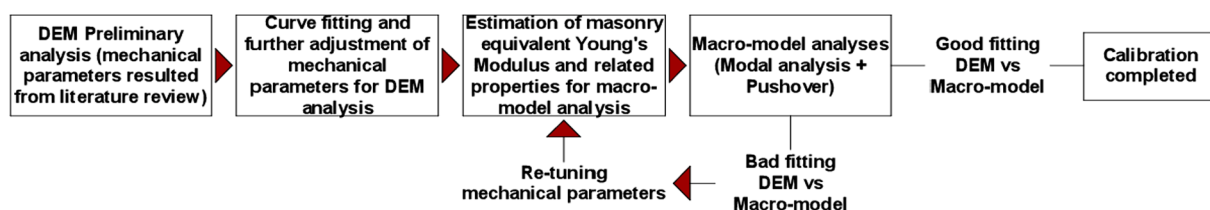


Fig. 12. Workflow calibration procedure.

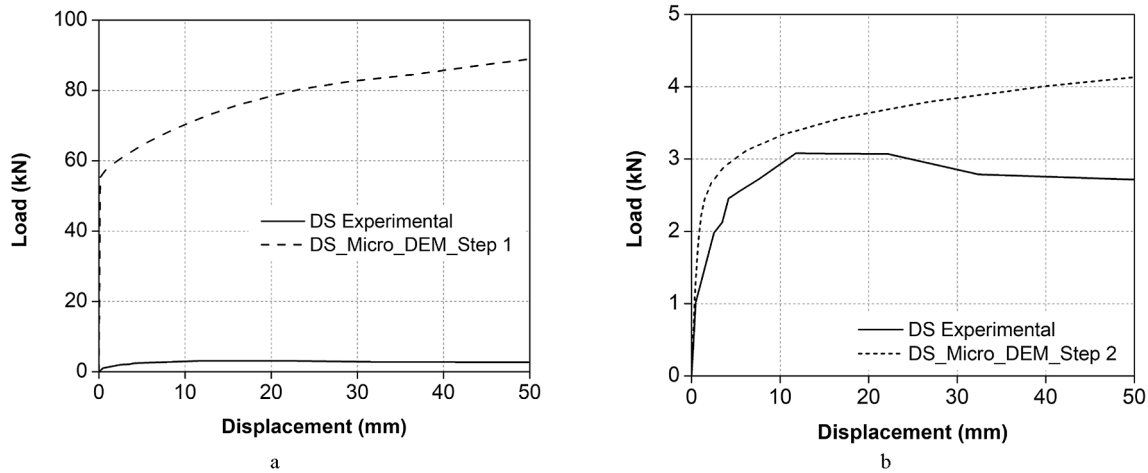


Fig. 13. Drystone masonry wall (DS) calibration procedure DS\_Micro\_DEM\_Step 1 (a) and DS\_Micro\_DEM\_Step 2 (b).

Table 4

Mechanical parameters to the simplified micro-model (DS).

Normal Stiffness ( $k_n$ )	2.00E+9 N/m <sup>3</sup> (2.40E+11 N/m <sup>3</sup> )
Shear Stiffness ( $k_s$ )	1.00E+9 N/m <sup>3</sup> (1.13E+11 N/m <sup>3</sup> )
Tensile Strength ( $f_t$ )	0 N/m <sup>2</sup> (4.03E+5 N/m <sup>2</sup> )
Cohesion ( $c$ )	0 N/m <sup>2</sup> (2.22E+3 N/m <sup>2</sup> )
Dilatancy ( $dl$ )	0 N/m <sup>2</sup>
Friction Angle ( $\phi_r$ )	10° (34°)

Table 5

Estimation of the Equivalent Young's Modulus (DS).

Itasca Manual [38]	Sarhosis [32]	Bui [29]	Gonen [53]
4.00E+8 N/m <sup>2</sup>	Not Available	3.93E+8 N/m <sup>2</sup>	4.00E+8 N/m <sup>2</sup>

Table 6

Initial (DS\_Macro\_FEM\_Step 1) and final (DS\_Macro\_FEM\_Step 2) properties macro-model drystone masonry wall.

Parameter	DS_Macro_FEM_Step 1	DS_Macro_FEM_Step 2
Young's Modulus (E)	3.98E+08 N/m <sup>2</sup>	2.95E+08 N/m <sup>2</sup>
Poisson ratio ( $\nu$ )	0.20	0.20
Density	2450 kg/m <sup>3</sup>	2450 kg/m <sup>3</sup>
Tensile strength ( $f_t$ )	39800 N/m <sup>2</sup>	934.20 N/m <sup>2</sup>
Mode I Fracture Energy (Gf1)	12 N/m	0.04 N/m
Compressive Strength ( $f_c$ )	398000 N/m <sup>2</sup>	93416.70 N/m <sup>2</sup>
Compr. Fracture Energy (Gfc)	637 N/m	149.47 N/m

which does not allow simulation of contact opening between the stones. Furthermore, from a computational standpoint, convergence problems occurred in DIANA whenever tensile strength, compressive strength, compressive fracture energy and mode I fracture energy values approached zero.

For this reason, in order to obtain a macro-model able to replicate the same assumptions characterising the DE model, namely no tension and no cohesion at the level of dry joints, the values of the input mechanical parameters, such as compressive fracture energy and Mode I fracture energy, have been set equal and with extremely low values (Table 6, column Step 2), ignoring the dependency of parameters such as tensile/compressive strength and compressive fracture energy from the masonry Young's Modulus.

Once, the mechanical parameters have been modified, it was observed that natural frequencies of vibration obtained in the macro-model reduced and approximate the values obtained in the micro-modelling approach.

The vibration modes resulting from numerical analyses have been qualitatively compared taking as a reference modes shapes and vibration

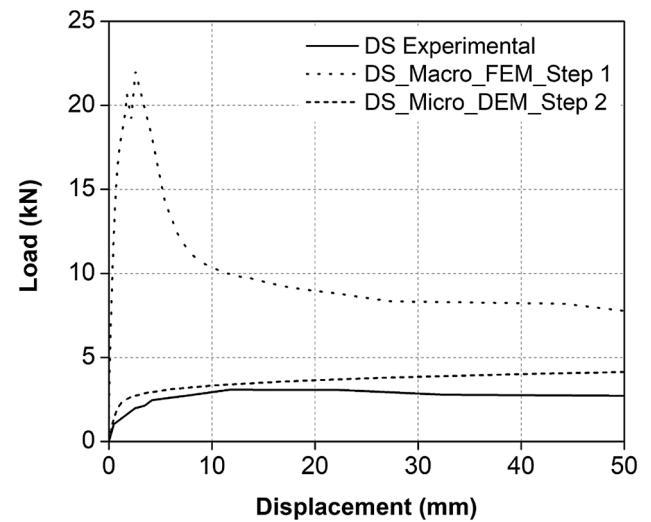


Fig. 14. Drystone masonry wall preliminary analyses macro-model (DS\_Macro\_FEM\_Step 1) vs DE-based simplified micro-model (DS\_Micro\_DEM\_Step 2).

frequencies those obtained via simplified DE-based micro-modeling. Successively, a quantitative evaluation of the level of correlation among vibration modes has been carried out by means of Modal Assurance Criterion (MAC), calculated using the following expression [71]:

$$MAC_{ij} = \frac{(\varphi_i^{num} \times \varphi_j^{num})^2}{(\varphi_i^{num} \times \varphi_j^{num})(\varphi_i^{exp} \times \varphi_j^{exp})} \quad (23)$$

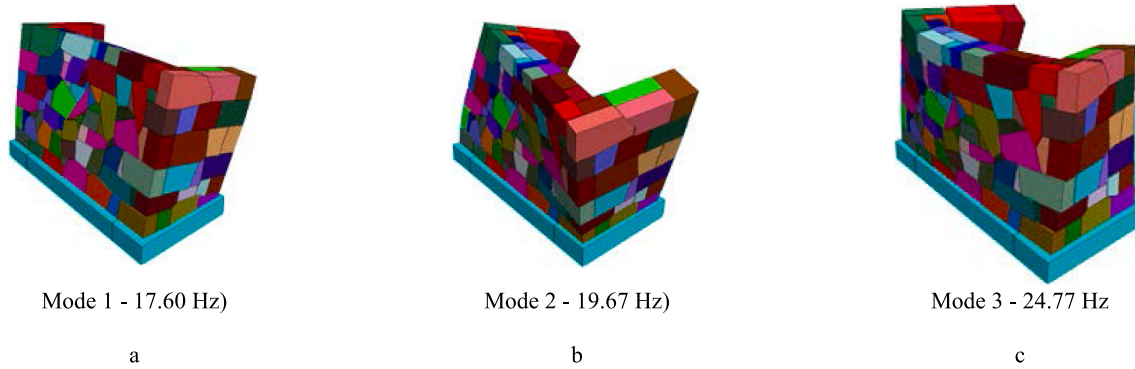
$i = 1, 2, \dots, n^{num}; j = 1, 2, \dots, n^{exp}$

where  $\varphi_i^{num}$  and  $\varphi_j^{exp}$  are the vectors of the modal components numerically and experimentally identified for  $n^{num}$  and  $n^{exp}$  modes, respectively.

Due to the lack of experimental data and being the main goal of this study to get an insight into the effectiveness of the modeling strategies adopted the input data referred to the experimental components has been obtained by simulating a dynamic identification test in 3DEC. Hence, a history of velocities of about 100 s corresponding to a white noise (frequency contents between 0 and 30 Hz) was applied at the base of the DE-base model [71].

The modal components obtained in 3DEC and post-processed in ARTEMIS software, have been used to assess the correspondence between DE-based models and FE-based models results in terms of mode shapes and frequencies of vibration. The peak values of frequency were

### Mode shapes and frequencies of vibration in simplified micro-model drystone masonry wall (3DEC)



### Mode shapes and frequencies of vibration in finite element macro-model drystone masonry wall (DIANA)

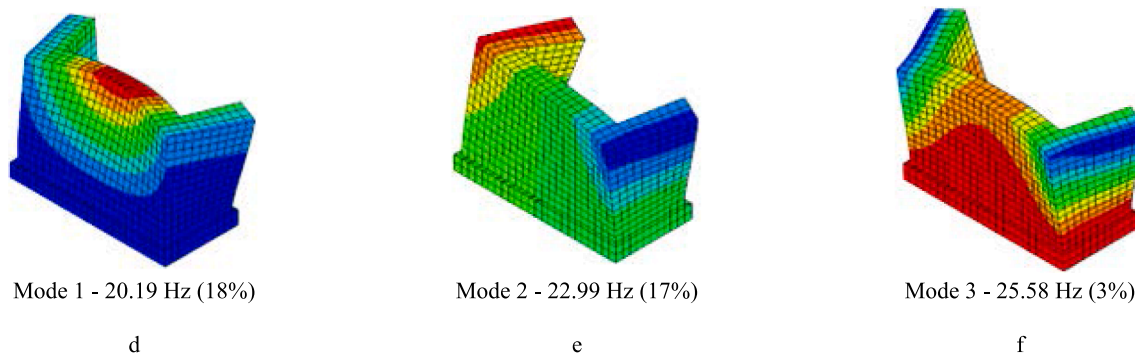


Fig. 15. DE micro-model drystone masonry wall Mode 1 (a), Mode 2 (b) and Mode 3 (c); FE macro-model drystone masonry wall Mode 1 (d), Mode 2 (d) and Mode 3 (c).

selected using Frequency Domain Decomposition (FDD) and Subspace Identification-Unweighted Principal Components (SSI-UPC) technique.

In the numerical macro-model, the third natural frequency is 11 % lower than the corresponding value obtained in the micro-model (DE model), whereas the first and second frequency of vibration have approximately the same value in both numerical models (Fig. 16).

Fig. 16 also shows the results of the natural frequencies and modes of vibration obtained for the micro-model prepared in DIANA. It should be stressed that the same mechanical properties used for the DE model have been adopted for the interface elements in the DIANA micro-model (Table 4), also considering the Mohr-Coulomb interface model. A good agreement can be also observed between DIANA and 3DEC simplified micro-models.

From Fig. 17, it is possible to analyse the force–displacement curves (control point) obtained from the calibrated macro-model (FEM) and micro-models (DEM and FEM) and compare them with the experimental results. It is observed that at this stage, there is a good consistency between macro-modelling and simplified micro-modelling. However, simplified micro-modelling curves tend to overestimate the experimental peak load, whereas the peak load obtained from the macro-model is slightly lower than the experimental maximum resisting force. The macro-model appears to properly capture the behaviour of the wall up to the end of the elastic regime. The post-peak behaviour shows a plateau in the FE simplified micro-model analysis, whereas, as previously stated, DE-based micro-model curve shows a plateau-like trend displaying slightly increasing load levels corresponding to a progressively increasing displacement level.

In the case of the macro-model, there is a slight decrease of the resistance, which is in more accordance with the experimental result. Additionally, the post-peak branch in the macro-model simulation has a decreasing trend more similar to the experimental results. Overall, it appears that the stiffness in the numerical models is higher than the

experimental test, which highlights a substantial loss of stiffness in the early stage of the test (for load level corresponding to approximately 1 kN).

Looking at the damage pattern corresponding to a displacement of 40 mm measured at the top mid span of the wall, it is possible to observe a good agreement between the simplified micro-model results (DIANA and 3DEC) and the experimental damage pattern. During the experimental out-of-plane test, the upper left portion of the façade wall (see Fig. 2a for reference) experienced a significant crack opening (Fig. 18a, b, c). The opening of this crack occurs at end of the linear behaviour of the wall, and it determines a progressive detachment of the façade from the left lateral wall.

This phenomenon has been captured in 3DEC (Fig. 18d, e, f) and the DIANA micro-models (Fig. 18l, m, n). It is also interesting to notice that the micro-models are very sensitive to the critical points related to the lack of interlocking of vertical joints, as both micro-models can capture the localized cracks at the main façade. Due to its intrinsic features, the macro-model is not able to capture this crack pattern related to the geometrical configuration of the stones. Despite this expected limitation, the macro-model is able to simulate the detachment phenomenon of the façade with respect to the lateral walls (Fig. 18g, h), revealed by the strain concentration at the connection between main façade and transversal walls.

### 6.2. Regular stone masonry wall (REGW)

Similar to what was carried out for the drystone masonry walls and following the steps from the calibration procedure summarised in Fig. 12, a preliminary analysis of the regular walls with mortar joints was carried out using 3DEC (e.g. the DE-based software). The initial mechanical properties adopted to characterise the interface elements of the DE models were previously defined and presented in Table 3 (see

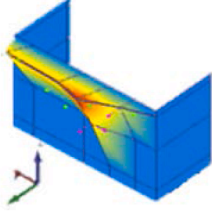
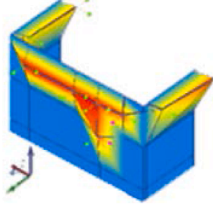
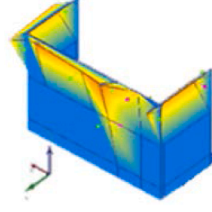
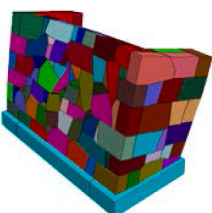
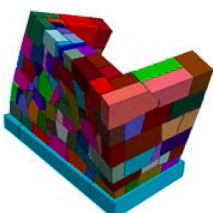
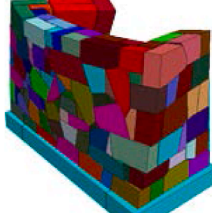
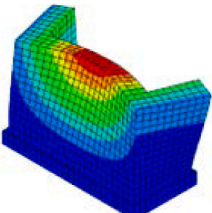
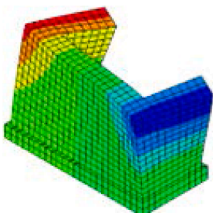
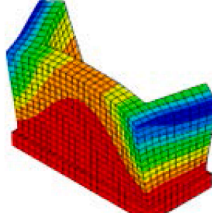
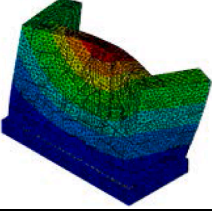
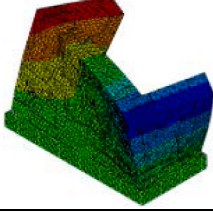
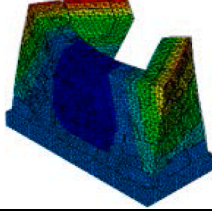
Mode shapes and frequencies of vibration simplified micro-model drystone masonry wall (Artemis)		
		
Mode 1 - 17.60 Hz	Mode 2 - 19.67 Hz	Mode 3 - 24.77 Hz
a	b	c
Mode shapes and frequencies of vibration simplified micro-model (3DEC) drystone masonry wall (DS)		
		
Mode 1 - 17.60 Hz	Mode 2 - 19.67 Hz	Mode 3 - 24.77 Hz
d	e	f
Mode shapes and frequencies of vibration macro-model (DIANA) drystone masonry wall (DS)		
		
Mode 1 - 17.50 Hz (2%) MAC - 0.93	Mode 2 - 19.20 Hz (1%) MAC - 0.83	Mode 3 - 22.99 Hz (-11%) MAC - 0.85
g	h	i
Mode shapes and frequencies of vibration simplified micro-model (DIANA) drystone masonry wall (DS)		
		
Mode 1 - 18.90 Hz (10%) MAC - 0.87	Mode 2 - 20.80 Hz (6%) MAC - 0.85	Mode 3 - 25.09 Hz (1%) MAC - 0.78
l	m	n

Fig. 16. Mode shapes and frequencies of vibration for all the modelling approaches considered (DS).

average values). As aforementioned, this table summarises the outcomes of the literature review carried out to gather reference values for the mechanical properties of the interface elements representing mortar joints.

Fig. 19 provides a comparison between the experimental load-displacement curve obtained in the out-of-plane test with

numerical response of the wall corresponding to first stage of the calibration procedure (REGW\_Micro\_DEM\_Step 1). It is also possible to compare it with the load-displacement diagram resulting from the iterative fitting process carried out in order to match the numerical and experimental data (REGW\_Micro\_DEM\_Step 2).

The first trial of the calibration analysis showed an overestimation in



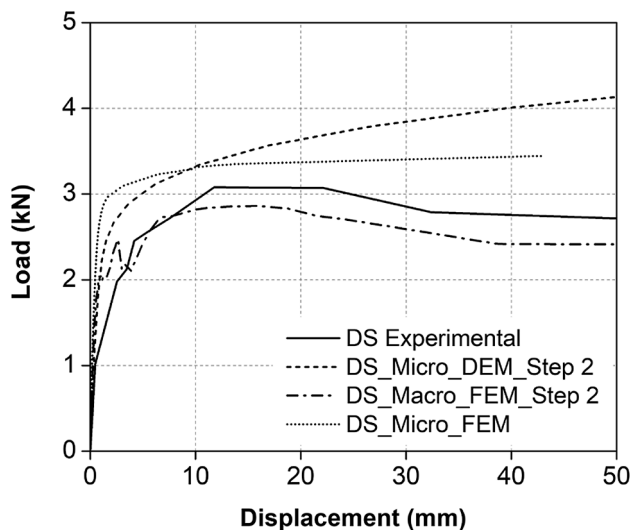


Fig. 17. Experimental and numerical Load vs Displacement curves drystone masonry wall (DS).

terms of peak load attained (approximately 60 kN). Similarly, the stiffness of the numerical model appears to be significantly higher when compared to the experimental result (see Fig. 19, REGW\_Micro\_DEM-Step 1 curve).

Hence, a refinement of the model's mechanical properties was carried out by adjusting stiffness parameters (assuming  $k_n = 2k_s$  as mentioned in Section 4) and tensile parameters assuming the cohesion equal to  $1.5 f_t$  (tensile strength), as mentioned in Section 5. The final parameters characterising the interface properties are presented in Table 7; it must be noted that the values in brackets refer to the input parameters used in the first trial of the calibration procedure reported in Table 3, Section 5. As previously stated regarding the drystone wall, both simplified micro-models (DE-based and FE-based model) have the same properties since both use a similar constitutive model for the interface elements (Mohr-Coulomb).

Once, the final values of normal and shear stiffness were correctly set, the updated normal stiffness was used to estimate the equivalent Young's Modulus of masonry to calculate other mechanical parameters as material input parameters for the macro-model analysis (using equations (14), (16), (19) and (21)). The values for the Young's Modulus of the drystone wall, calculated based on the different formulations are summarised in Table 8, and the average value, stands at  $8.47E+8 \text{ N/m}^2$  (847 MPa). Also for this type of masonry, it was not possible to use the formulation proposed by Sarhosis [32] due to the absence of reference values related to the Young's modulus of mortar.

Table 9 presents the final values adopted for the macro-modelling approach, estimated using equations from 9 to 12 and based on the average equivalent Young's Modulus value ( $8.47E+8 \text{ N/m}^2$ ). The consistency of the properties, estimated for each modelling approach, has been assessed by means of a modal analysis to compare mode shapes and natural frequencies of vibration. The numerical results have been also compared to the experimental data obtained from the dynamic identification test performed on the masonry wall (REGW).

As Fig. 20 illustrates, good consistency can also be observed in terms of natural frequencies of vibration and mode shapes. The assessment of the correspondence among modal components has been carried out similarly to what mentioned in Section 6.1 regarding the drystone wall (DS), hence applying the Modal Assurance Criterion, taking as a reference the results obtained after simulating an dynamic identification test on the regular wall (REGW) in 3DEC.

In the simplified DE-based micro-model, the first frequency of vibration is 6 % higher than the corresponding experimental value

(Fig. 20d) and conversely, the second frequency of vibration is 7 % lower than the corresponding experimental value (Fig. 20e). A similar trend was found for both the macro-model analysis and FE micro-model analysis. The macro-model presents natural frequencies values 5 % higher and 8 % lower than the experimental data for the first and second frequencies respectively (Fig. 20g and Fig. 20h), whereas the FE-based micro-model shows an increase equal to 5 % for the first natural frequency and a decrease equal to 12 % for the second frequency when compared to the experimental results (Fig. 20i and Fig. 20m).

Fig. 21 presents the load–displacement diagrams resulting from the pushover analyses performed using the different calibrated modelling approaches. All the considered modelling approaches yielded similar results in terms of initial stiffness.

The FE-based micromodel led to a peak load of approximately 40 kN, which is slightly lower in comparison to the peak load achieved in the analysis carried out with DE-based simplified micro-model (peak load around 43 kN). In both cases the value is very close to the experimental peak load of 43.50 kN.

A higher difference in terms of peak load was found for the macro-model. In this case, the peak load is around 15 % lower than the experimental peak load. The post-peak behaviour in both simplified micro-modelling approaches (DE-based and FE-based) shows a plateau characterised by almost no increasing load for increasing lateral displacements. On the other hand, the macro-model load–displacement curve is characterised by an abrupt decrease of the lateral resistance of the wall after reaching the peak load.

The damage pattern in the DE and FE simplified micro-models (corresponding to a displacement level equal to 40 mm) is also similar. Diagonal cracks open in the façade wall resulting in a progressive increase of the detachment between the façade and the lateral walls (Fig. 22d–e–f and Fig. 22l–m–n). For a higher level of displacement, it is possible to observe a gradual sliding phenomenon affecting the top masonry horizontal layer.

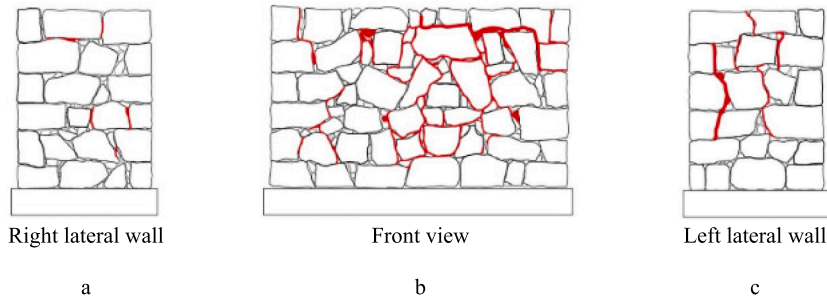
Looking at the macro-model strain concentration (corresponding to a displacement level equal to 40 mm), it is possible to conclude that damage mostly affects the connection between lateral walls and façade, as well as the upper central part of the main façade. It is possible to observe that the strain concentration coincides with the diagonal cracks that developed in both simplified micro-models (Fig. 22g–h). Moreover, the highest strain concentration in the upper part of the façade shows a good consistency with the outcome related to the micro-model-based analyses, which show higher displacements of the upper masonry layers.

Regarding the experimental damage pattern (Fig. 22a–b–c), the numerical models are also roughly able to represent the damage, even if the crack asymmetry could not be captured by DE-based simplified micro-model and FE-based macro-model. On the other hand, in the FE-based simplified micro-model the occurrence of an asymmetrical damage pattern was slightly captured (Fig. 22i–l–m).

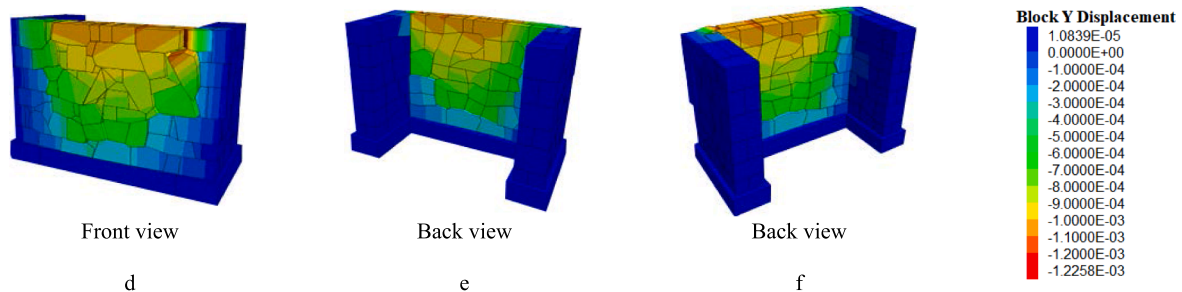
Therefore, it is possible to state that the selected numerical approaches proved to be reliable in assessing the out-of-plane performance of the selected experimental reference. In particular, the micro-model approaches (DE-based and FE-based) provided a good estimation of the out-of-plane performance of the regular wall (REGW) both in terms of peak load attained and initial stiffness. The post peak branch, however, is characterised by a plateau (Fig. 21, REGW\_Micro\_DEM\_Step 2 curve and REGW\_Micro\_FEM curve) which overestimates the displacement capacity of the walls, when compared with the experimental results. Nevertheless, the main advantage of both micro-model analyses lies in the considerable accuracy in simulating the final damage pattern.

On the other hand, the macro-model analysis showed an expected lack of accuracy in simulating asymmetrical damage patterns. This is essentially due to the specific characteristic of the modelling approach which represents complex geometries in a simplified configuration. Therefore, since acting loads and boundary conditions are symmetrically applied to the model the corresponding displacements and deformations will spread symmetrically as well.

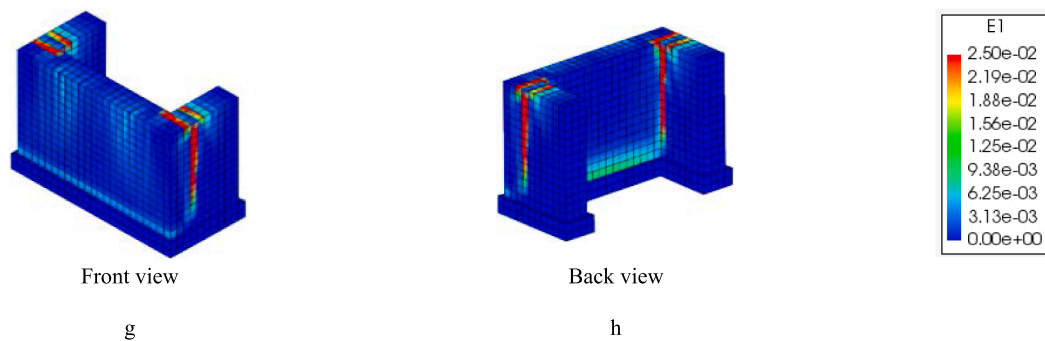
**Experimental damage pattern drystone masonry wall**



**Damage pattern micro-model drystone masonry wall (3DEC) – Displacement level 40 mm**



**Damage pattern macro-model drystone masonry wall – Displacement level 40 mm**



**Damage pattern micro-model drystone masonry wall (DIANA) – Displacement level 40 mm**

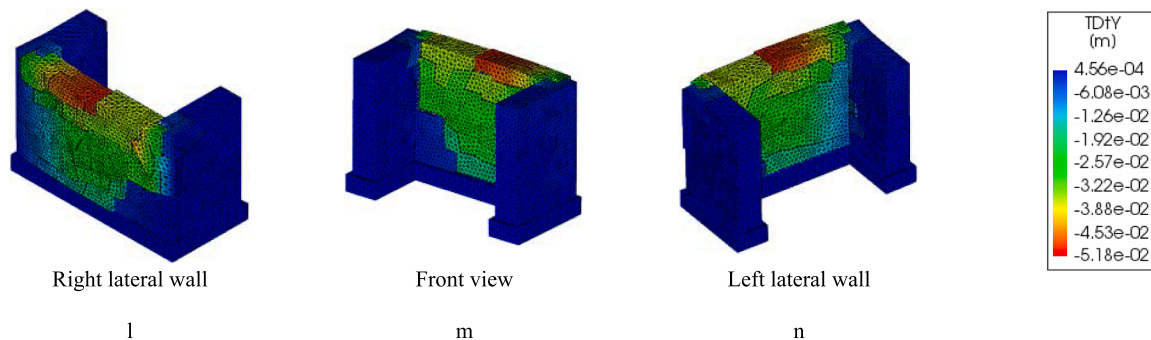


**Fig. 18.** Numerical and experimental damage pattern drystone masonry wall.

Obviously, depending on the aim of a specific study and depending on the extent of the structure to be analysed, one procedure can be preferred to another. Overall, the macro-model and DE-based micro-model approaches provided good results with an effective balance between accuracy and computational effort. In particular, the DE-based analysis provided a better approximation of the damage pattern and a considerably smaller computational demand if compared to FE-based micro-model, which in any case, provided similar results. However,

the preparation of the 3D geometry of DE-based models is significantly more time consuming than FE-based macro-models.

To summarise, macro-model is the most suitable option for practice-oriented engineering activities involving the analysis of large structures. A viable alternative could be DE-based analyses whenever a better understanding of specific damage mechanisms is required, and the morphology of the wall is simple to model and/or the model can accept simplifications of the morphology of the masonry bond and geometry.

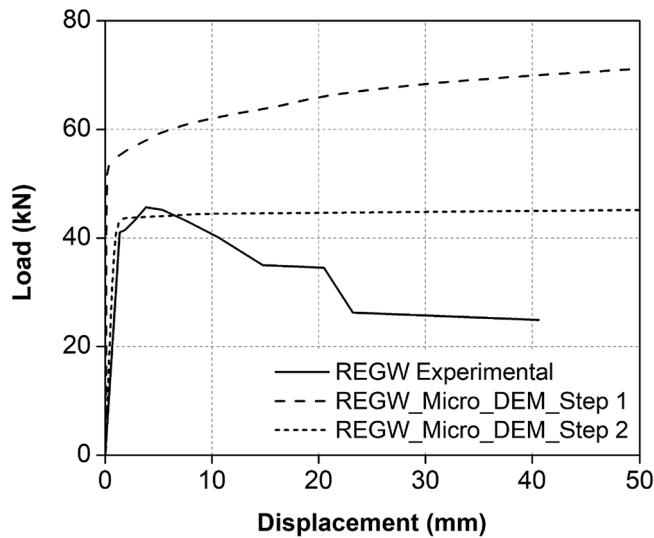


Fig. 19. Regular masonry wall (REGW) calibration procedure step 1 (a) and step 2 (b).

Table 7

Mechanical parameters simplified micro-model (REGW).

Normal Stiffness ( $k_n$ )	4.20E+9 N/m <sup>3</sup> (2E+12 N/m <sup>3</sup> )
Shear Stiffness ( $k_s$ )	2.10E+9 N/m <sup>3</sup> (9E+11 N/m <sup>3</sup> )
Tensile Strength ( $f_t$ )	1.50E+5 N/m <sup>2</sup> (1.10E+5 N/m <sup>2</sup> )
Cohesion ( $c$ )	1.90E+5 N/m <sup>2</sup> (4.85E+5 N/m <sup>2</sup> )
Dilatancy ( $dl$ )	0 N/m <sup>2</sup>
Friction Angle ( $fr$ )	33°

Table 8

Equivalent Young's Modulus values (REGW).

Equivalent Young's Modulus estimation (Regular Masonry Wall with mortar joints – REGW)			
Itasca Manual [38]	Sarhosis [32]	Bui [29]	Gonen [53]
8.20E+8 N/m <sup>2</sup>	Not Available	8.20E+8 N/m <sup>2</sup>	9.00E+8 N/m <sup>2</sup>

FE-based micro-model analyses, which have a higher computational demand, remain a good option to model smaller portions of structures or to simulate experimental testing procedures involving reduced-sized specimens.

### 6.3. Assessment of the onset out-of-plane load via updated analytical formulation

Starting from the experimentally observed damage patterns, a limit analysis based on an updated formulation proposed in Casapulla [3] has been carried out in order to estimate the load level that activates the failure mechanism in both drystone (DS) and regular stone masonry wall (REG).

DS and REGW damage mechanisms involve the overturning of a portion of the façade combined to the detachment of the façade itself from the lateral walls. Three possible failures modes have been considered namely, a simple rocking (Mechanism A), a compound rocking (Mechanism B) and a horizontal flexure (Mechanism D), see also

Table 9

Mechanical parameters macro-modelling approach (REGW).

Young's Modulus ( $E$ )	8.47E+8 N/m <sup>2</sup>
Poisson ratio ( $\nu$ )	0.39
Density	2495 kg/m <sup>3</sup>
Tensile strength ( $f_t$ )	8.47E+4 N/m <sup>2</sup>
Mode I Fracture Energy ( $G_{fI}$ )	12 N/m <sup>2</sup>
Compressive Strength ( $f_c$ )	8.47E+5 N/m <sup>2</sup>
Compr. Fracture Energy ( $G_{fc}$ )	1355 N/m

Table 1, Mechanism A, B and D reported in [3].

Fig. 23a, b, c shows the scheme of external and internal actions in all the mechanisms considered in the limit analysis procedure as well as a 3D schematic view (Fig. 23d, e, f).

It is noteworthy to point out that the notation and the nomenclature adopted for the input parameters used in the limit analysis are the same of those proposed in Casapulla [3]. Additionally, the basic assumptions considered to obtain a structural scheme as close as possible to the load configuration and the experimental setup of the out-of-plane test are the following.

- The restraining action due to beam connection ( $\mu Q_{fo}$ ) is neglected since this type of load is not present in the experimental configuration. A uniformly distributed load equal to 5.48 kN/m has been considered acting on top of each tested wall. This value resulted from the ratio between the total external vertical load acting on the top of the tested walls (20 kN in both DS and REGW) and the extension of the centroidal axis of the plan view of the wall (equal to 3.65 m, see Fig. 2a).
- The number of masonry courses in REGW is 6, whereas the number of courses between the top of the wall and the hinge O ( $n_k$ ) is set equal to 4. In Mechanism B, the number of courses crossed by the crack at the  $i^{\text{th}}$  storey ( $n_c$ ) is set equal to 4.
- The average height of stone units is set equal to 0.225 m, the thickness is set equal to 0.15 m considering a two-leaf wall with total thickness of 0.30 m, and the average length of stone units is set equal to 0.29 m. The resulting staggering ratio ( $\nu$ ) is 0.144 m. Based on these assumptions, the estimated maximum admissible crack angle ( $\alpha_b$ ) in compliance with the staggering ratio is approximately 26°. In Mechanism B, a value of 13° has been set for the crack inclination angle ( $\alpha_c$ ), hence considering an average contribution of the frictional forces to the failure mechanism.
- To overcome issues related to the irregular geometrical configuration in DS, the same assumptions related to stone units' dimensions and staggering ratio have been adopted.
- The friction coefficients ( $f$ ) have been computed starting from the friction angle values presented in Table 4 and Table 7 for the drystone wall (DS) and regular stone masonry wall (REGW) respectively. The load factor corresponding to the selected failure mechanism can be estimated as follows for DS and REGW [3]:

$$\lambda_{r,o-A} = \frac{W_{Ai}X_{Ai} + \mu Q_{fi}Z_{Q_{fi}} + Q_{fi}X_{Q_{fi}}}{W_{Ai}Z_{W_{Ai}} + Q_{fi}Z_{Q_{fi}}} + \frac{n_s(F_{gi}Z_{F_{gi}} + F_{qi}Z_{F_{qi}})}{W_{Ai}Z_{W_{Ai}} + Q_{fi}Z_{Q_{fi}}} \quad (24)$$

$$\lambda_{r,o-B} = \frac{W_{Ai}X_{Ai} + \mu Q_{fi}Z_{Q_{fi}} + Q_{fi}X_{Q_{fi}} + n_s(W_{Di}X_{W_{Di}} + \omega(F_{ji} + Q_{si}X_{Q_{si}}))}{W_{Ai}Z_{W_{Ai}} + Q_{fi}Z_{Q_{fi}} + n_s(W_{Di}Z_{W_{Di}} + Q_{si}Z_{Q_{si}})} \quad (25)$$

$$\lambda_{1,r,o-D} = \frac{2(W_A Z_{W_A} + \mu Q_{fA} Z_{Q_{fA}}) + (W_B Z_{W_B}) + (\mu Q_{fB} Z_{Q_{fB}}) + 4k(T_{o_s} + T_{o_q})}{2(W_A Y_{W_A} + Q_{fA} Y_{Q_{fA}}) + (W_B Z_{W_B} + Q_{fB} Y_{Q_{fB}}) + 2kd_0(W_A + W_B + Q_{fA} + Q_{fB})} \quad (26)$$

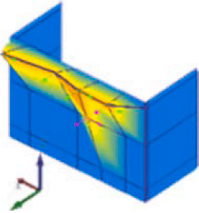
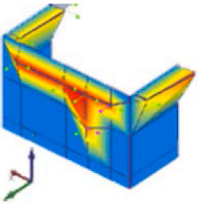
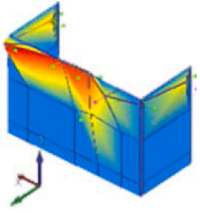
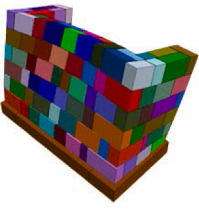
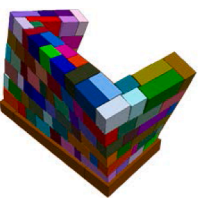
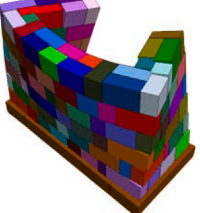
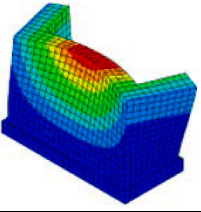
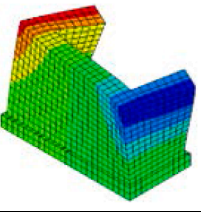
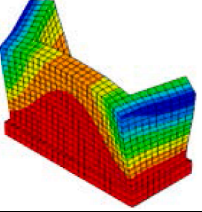
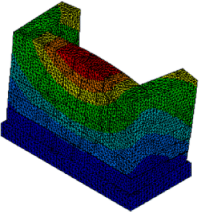
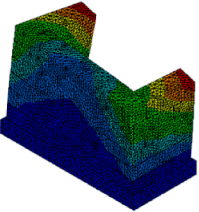
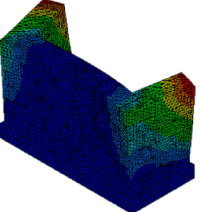
Mode shapes and frequencies of vibration simplified micro-model regular masonry wall (Artemis)		
		
a	b	c
Mode 1 – 28.35 Hz	Mode 2 – 32.45 Hz	Mode 3 – 36.15 Hz
Mode shapes and frequencies of vibration simplified micro-model (3DEC) regular masonry wall (REGW)		
		
d	e	f
Mode 1 – 28.35 Hz (6%)	Mode 2 – 32.45 Hz (-7%)	Mode 3 – 36.15 Hz
Mode shapes and frequencies of vibration macro-model regular masonry wall (REGW)		
		
g	h	i
Mode 1 – 28.03 Hz (5%) MAC – 0.91	Mode 2 – 32.06 Hz (-8%) MAC – 0.84	Mode 3 – 35.71 Hz MAC – 0.79
Mode shapes and frequencies of vibration simplified micro-model (DIANA) regular masonry wall (REGW)		
		
l	m	n
Mode 1 – 28.01 Hz (5%) MAC – 0.88	Mode 2 – 30.73 Hz (-12%) MAC – 0.83	Mode 3 – 36.52 Hz MAC – 0.81

Fig. 20. Mode shapes and frequencies of vibration for all the modelling approaches considered (REGW).

For the sake of brevity, the reader is referred to Casapulla [3], for a more detailed definition of the variables common to the selected mechanisms. These formulations refer to N-storey buildings, considering the storeys indexed by the variable  $i = 1, 2, 3, \dots, N$ , from the top to the ground storeys. Since the structural scheme considered for both walls has just 1 floor,  $i$  is equal to 0 ( $i = 0$ ).

$W_{Ai}$  (external action due to self-weight),  $Q_{fi/si}$  (overload on the façade/lateral walls),  $F_{gi}$  (maximum frictional resistance due to the

contribution of the self-weight) and  $F_{qi}$  (maximum frictional resistance due to the contribution of the overload) together with their lever arms (X, Y and Z) are calculated according to the equations proposed in [3] (see Table 3, 4 and 6 for Mechanism A, B and D respectively).

$S_{oj}$  and  $T_o$  are the shear and torsion contributions, respectively, which characterize Mechanism D [3], computed taking into account a reduction of contact interfaces corresponding to a corrective coefficient  $k$  set equal to 0.5.

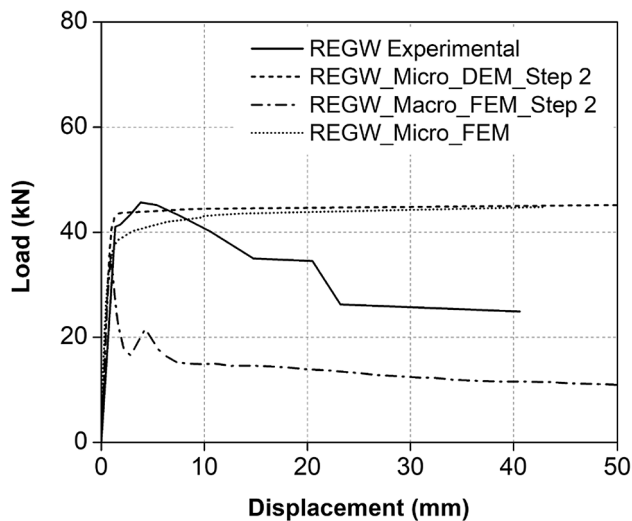


Fig. 21. Experimental and numerical Load vs Displacement curves regular masonry wall (REGW).

Finally, due to the absence of specific information regarding the tested drystone wall (DS), the same density value as the REGW has been assigned. It must not be overlooked that the actual density value for this type of masonry is lower than that considered, hence, leading to an analytical value closer to those related to experimental, FE-macro model and DE-model results.

The load factor and its corresponding load are reported in Table 10 for both DS and REGW. The table reports the percentage difference between the Light Damage Load and the Limit Analysis Load for each mechanism considered, this value is presented in round brackets while the letter A, B and D refer to the mechanism considered (see column Light Damage Load in Table 10).

The analytically estimated load has been compared to the Light Damage Load which corresponds to the load level in the so-called Light Damage limit state, according to the definition proposed in [72], which correlates the beginning of cracking phenomena in masonry structures to a reduction of 2 % of the initial stiffness.

Moreover, Load Factor and Limit Analysis Load analytically computed are shown in the last 2 columns. The onset load (Limit Analysis Load) is computed by multiplying the load factor derived from the limit analysis procedure ( $\lambda$ ), by the mass of the macro-element related to the mechanism selected and by the gravitational acceleration ( $\approx 10 \text{ m/s}^2$ ).

In DS wall, despite Mechanism B is the prevailing failure mode experimentally observed, the onset load related to the horizontal flexure (Mechanism D) is closer to the experimental outcome. On the other hand, DE-base micro-model results show a good consistency between the observed failure mode, namely horizontal flexure (Mechanism D) and the loads numerically and analytically computed, with a percentage difference of 26 % (the lowest among the collapse mechanisms considered), see Table 10.

FE-based micro-model is characterized by a horizontal flexure prevailing failure mode. However, a better agreement in terms of load level is shown when considering a simple rocking mechanism (Mechanism A).

FE-based macro-model presents a simple rocking failure, but in terms of load level the lowest difference between numerical and analytical results is detectable when Mechanism D is considered (14 %).

In REGW, experimental and analytical results show a good agreement both in terms of collapse mechanism detected (Mechanism B) and in terms of load levels attained (lowest percentage difference among the mechanisms considered, approximately 23 %), see Table 10.

DE-based micro-model results highlight a good consistency between load levels attained when Mechanism B is considered, even though the

observed failure mode is a horizontal flexure. A similar trend is detectable looking at the result of the FE-based micro-model.

However, in FE-based macro-model the percentage difference between the onset load related to Mechanism A is 53 % if compared to the numerically estimated load. In this case, despite being simple rocking the observed failure mode, from a load level standpoint the best approximation of the numerical results is provided by the limit analysis carried out assuming a collapse due to a compound rocking behaviour.

Overall, in the case of the regular wall (REGW), the mechanism experimentally observed (Mechanism B, compound rocking) is consistent with the results obtained by means of limit analysis. Analytical results obtained by assuming a compound rocking failure mechanism proved to be sufficiently accurate when compared to the numerical results, although some discrepancies between observed and assumed failure modes can be detected.

On the other hand, DS wall's results display more heterogeneity. The experimentally observed failure mode is compound rocking (Mechanism B), but the value of onset load closer to the Light Damage State load refers to the limit analysis carried out assuming a horizontal flexural failure. Among the numerical methods considered, FE-based micro-model provided a good fitting of the analytical results. Indeed the intrinsic complexity of the physical phenomena involved in the simulation of the behavior of the drystone masonry wall (mostly frictional action influenced by the geometrical configuration of the masonry bond), makes it difficult to obtain a perfect fitting among experimental, numerical, and analytical results.

## 7. Conclusions

This study presents a comparison among different numerical modelling approaches applied for the simulation of the out-of-plane behaviour of two-leaf stone masonry walls, namely finite element-based macro/micro modelling and distinct element based micro modelling.

The numerical results were compared with experimental results from out-of-plane tests previously carried out. The walls have different masonry bond and constructive systems, namely one wall is a drystone masonry wall (DS), and the other is a roughly regular masonry bond wall with mortar joints (REGW). The main aspects arising from this study are:

- (1) the calibration procedure of the models, carried out based on reference values of mechanical properties and empirical equations available in the literature, highlighted a lack of consistency in estimating the mechanical properties of the drystone wall (DS) mainly when a finite element based macro modelling approach is considered, whereas a better agreement between empirical expression and final mechanical properties has been obtained in the regular wall with mortar joints (REGW). The empirical expression found in the literature are, in fact, mainly targeted for masonry walls with mortar joints, hence, further analyses could be carried out to fill this gap related to the parameter estimation of drystone masonry.
- (2) The masonry bond geometrical configuration strongly influenced the overall out-of-plane response of the selected walls. The regular wall with mortar joints (REGW) showed a higher strength capacity and a higher stiffness level compared to the drystone wall (DS), due to, among other aspects, a better interlock among stone masonry units.
- (3) Despite its intrinsic limitations (e.g. inability in simulating asymmetrical crack patterns and inability to fully capture the frictional phenomena characterizing the drystone masonry wall), finite element based macro modelling approach proved to be reliable in identifying the areas of the walls which may be display higher level of damages. On the other hand, both finite element based, and distinct element based micro modelling approaches

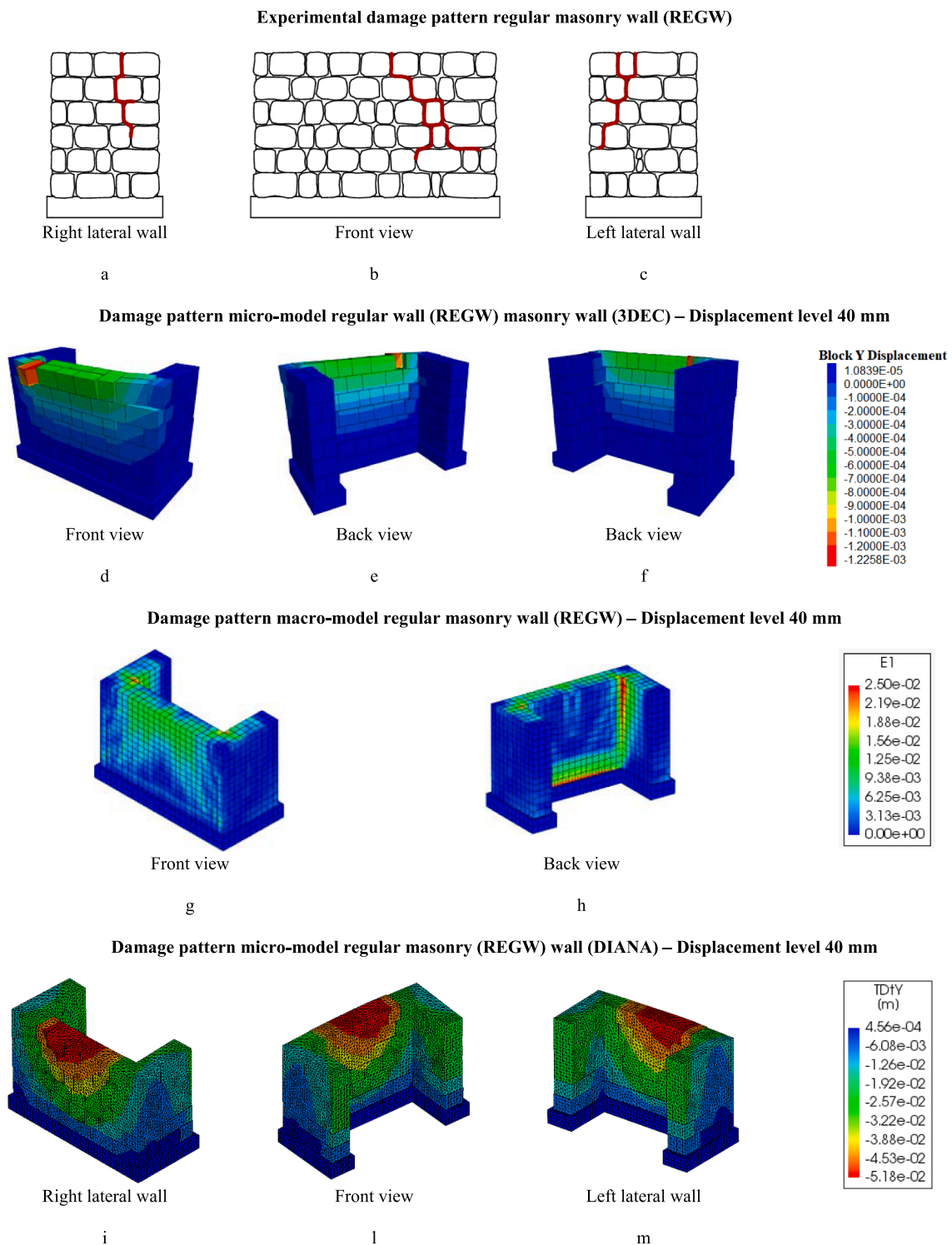


**Fig. 22.** Experimental and numerical damage pattern regular masonry wall (REGW).

provided a more accurate estimation of the crack patterns of the walls under study.

- (4) Taking into account the aforementioned considerations the choice of a specific modelling approach should take into account the computational effort and the time required to build the geometrical model to be used in the software package selected to carry out the numerical simulation. To this end, it is worth to mention that a finite element based micro-model pushover analysis required a run time higher than 7 days, whereas the run

time for a distinct element based pushover analysis required less than 30 min; a similar computational effort (average of 30 min) characterised the finite element based macro-model analyses carried out.

Additionally, one of the most time-consuming tasks for the finite element based micro-model is the contact detection and the application of interface elements in DIANA software. This task had to be carried out manually for all the masonry units (overall duration ranging from 5 to

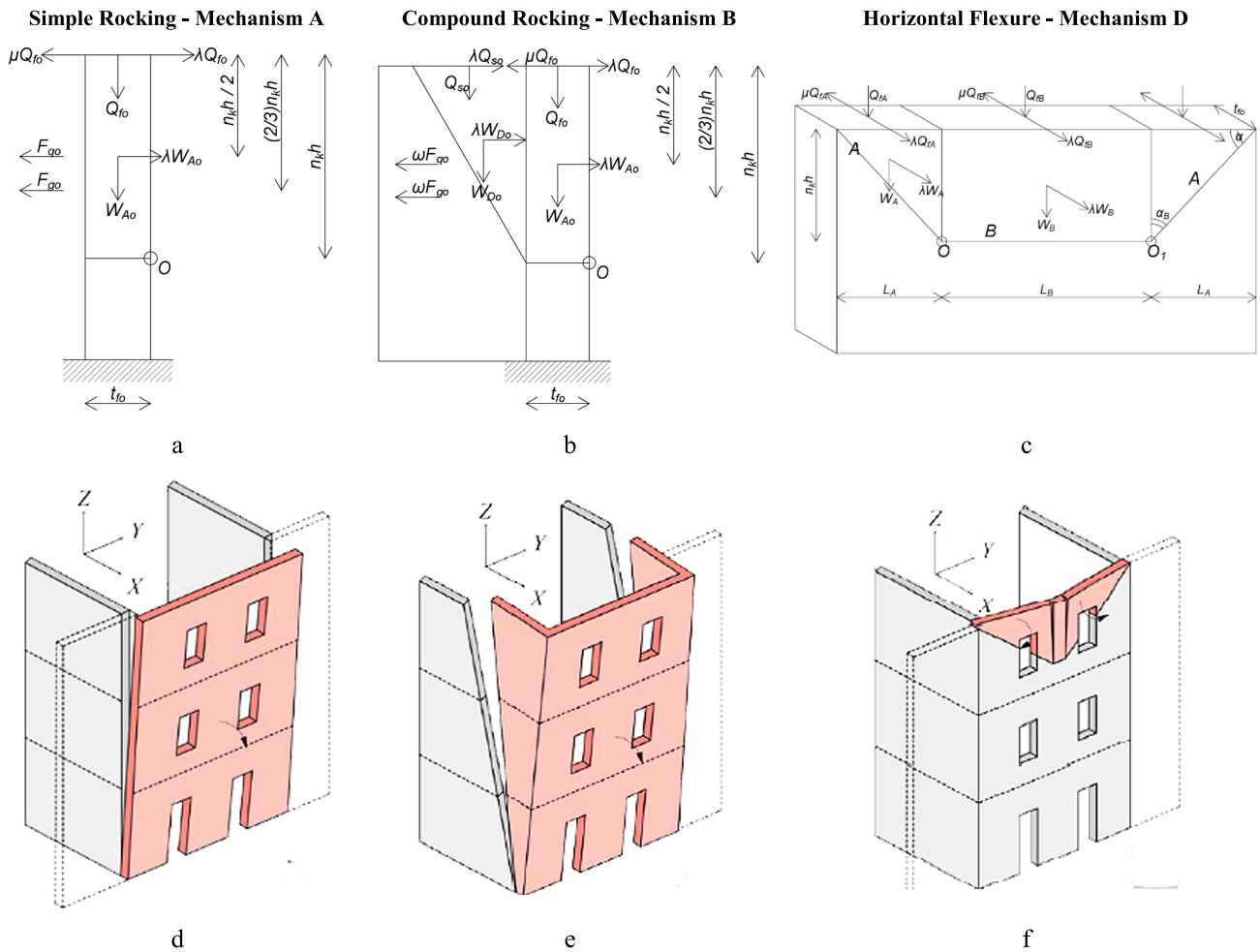


Fig. 23. Scheme of internal and external actions in simple rocking (a), compound rocking (b) and horizontal flexure mechanism(c); 3D schematic view of simple rocking (d), compound rocking (e) and horizontal flexure (e) mechanism, . adapted from [3]

Table 10  
Onset load for the out-of-plane mechanism estimated based on experimental, analytical and numerical results.

	Initial Stiffness (kN/mm)	Initial Displ. (mm)	Prevalent Collapse Mechanism Observed	Light Damage Load (kN)	Load Factor ( $\lambda$ )	Limit Analysis Load (kN)
DS Experimental	2.15	0.47	Compound Rocking - B	0.99 (50 %) – A0.99 (71 %) – B0.99 (2 %) – D	Mech. A = 0.09 Mech. B = 0.083	Mech. A = 2.01 Mech. B = 3.38 Mech. D = 0.97
DS_Micro_DEM_Step 2	2.80	0.48	Horizontal Flexure - D	1.31 (35 %) – A1.31 (61 %) – B1.31 (26 %) – D	0.302 Mech. D = 0.083	
DS_Macro_FEM_Step 2	3.10	0.57	Simple Rocking - A	0.83 (59 %) – A0.83 (75 %) – B0.83 (14 %) – D		
DS_Micro_FEM	4.18	0.50	Horizontal Flexure - D	2.05 (2 %) – A2.05 (39 %) – B2.05 (53 %) – D		
REGW Experimental	29.80	0.33	Compound Rocking - B	9.63 (46 %) – A9.63 (23 %) – B9.63 (73 %) – D	Mech. A = 0.231 Mech. B = 0.391	Mech. A = 5.16 Mech. B = 7.46 Mech. D = 1.45
REGW_Micro_DEM_Step 2	46.09	0.22	Horizontal Flexure - D	9.93 (48 %) – A9.93 (25 %) – B9.93 (74 %) – D	0.270	
REGW_Macro_FEM_Step 2	46.42	0.24	Simple Rocking - A	10.91 (53 %) – A10.91 (32 %) – B10.91 (76 %) – D		
REGW_Micro_FEM	43.08	0.23	Horizontal Flexure - D	9.71 (47 %) – A9.71 (23 %) – B9.71 (73 %) – D		

10 h). Conversely, in 3DEE (DE-based software), the detection and the definition of the interface elements is a semi-automatic procedure (overall duration less than 15 min depending on the geometrical complexity of the model), carried out by means of specific code-based inputs that considers the configuration of the CAD 3D model.

In conclusion, among the finite element based modelling approaches considered in this study, macro-modelling represents the best solution for practice-oriented engineering activities since it provides a good compromise between accuracy and computational effort. On the other hand, finite element based micro-modelling provided accurate results but with a considerable computational effort. Overall, this approach is a viable choice whenever experimental tests on small-scale specimens need to be simulated, but it is not an effective option when it comes to analyse particularly large models. On the other hand, distinct element based micro modelling proved to be effective in simulating the overall behaviour of both drystone (DS) and regular wall (REGW) with a reasonable run time for all the analyses performed, hence representing a viable alternative to both FE-based modelling approaches.

### CRedit authorship contribution statement

**Antonio Murano:** Conceptualization, Methodology, Formal analysis, Data curation, Writing - original draft. **Anjali Mehrotra:** Conceptualization, Supervision, Writing - review & editing. **Javier Ortega:** Conceptualization, Supervision, Writing - review & editing. **Hugo Rodrigues:** Supervision, Writing - review & editing. **Graça Vasconcelos:** Supervision.

### Declaration of Competing Interest

The authors declare that they have no known competing financial interests or personal relationships that could have appeared to influence the work reported in this paper.

### Data availability

Data will be made available on request.

### Acknowledgements

This work was partly financed by FCT/MCTES through national funds (PIDDAC) under the R&D Unit Institute for Sustainability and Innovation in Structural Engineering (ISISE), under reference UIDB/04029/2020.

This work is financed by national funds through FCT - Foundation for Science and Technology (Portugal), under grant agreement SFRH/BD/147708/2019 attributed to the 1<sup>st</sup> author.

### References

- Roca P, Lourenço PB, Gaetani A. *Historic construction and conservation. Materials, systems and damage*. New York: Routledge; 2019.
- Carocci C. Guidelines for the safety and preservation of historical centres in seismic areas. In: *Historical constructions - possibilities of numerical and experimental techniques*; 2001. p. 145–66.
- Casapulla C, Argiento L, Maione A, Speranza E. Upgraded formulations for the onset of local mechanisms in multi-storey masonry buildings using limit analysis. *Structures* 2021;31:380–94. <https://doi.org/10.1016/j.istruc.2020.11.083>.
- Casapulla C, Argiento L. The comparative role of friction in local out-of-plane mechanisms of masonry buildings. Pushover analysis and experimental investigation. *Eng Struct* 2016;126:158–73. <https://doi.org/10.1016/j.engstruct.2016.07.036>.
- D'Ayala DF, Speranza E. Definition of collapse mechanisms and seismic vulnerability of historic masonry buildings. *Earthq Spectra* 2003;19(3):479–509. <https://doi.org/10.1193/1.1599896>.
- Vlachakis G, Vlachaki E, Lourenço PB. Learning from failure: Damage and failure of masonry structures, after the 2017 Lesvos earthquake (Greece). *Eng Fail Anal* 2020;117:104803. <https://doi.org/10.1016/j.engfailanal.2020.104803>.
- Giuffrè A. *Lettura sulla meccanica delle murature storiche*. Roma: Eizioni Kappa; 1991.
- Vitruvio Pollione M. *De Architectura*. Pordenone.
- Rondelet J-B. *Trattato teorico e pratico dell'arte di edificare*. Mantova; 1834.
- Borri A, Corradi M, Castori G, De Maria A. A method for the analysis and classification of historic masonry. *Bull Earthq Eng* 2015;13(9):2647–65. <https://doi.org/10.1007/s10518-015-9731-4>.
- D'Altri AM, Sarhosis V, Milani G, Rots J, Cattari S, Lagomarsino S, Sacco E, Tralli A, Castellazzi G, de Miranda S. Modeling strategies for the computational analysis of unreinforced masonry structures: review and classification, Vol. 27, no. 4. Springer Netherlands; 2020.
- Asteris PG, Tzamtzis AD. On the use of a regular yield surface for the analysis of unreinforced masonry walls. *Electron J Struct Eng* 2003;3:23–42.
- Lourenço P. Recent advances in Masonry modelling: micromodelling and homogenisation. In: *Multiscale modeling in solid mechanics: computational approaches*. London: Imperial College Press; 2009. p. 251–94.
- Bartoli G, Betti M, Vignoli A. A numerical study on seismic risk assessment of historic masonry towers: a case study in San Gimignano. *Bull Earthq Eng* 2016;14(6):1475–518. <https://doi.org/10.1007/s10518-016-9892-9>.
- Orlando M, Betti M, Spinelli P. Assessment of structural behaviour and seismic retrofitting for an Italian monumental masonry building. *J Build Eng* 2020;29:101115. <https://doi.org/10.1016/j.jobe.2019.101115>.
- Orlando M, Becattini G, Betti M. Multilevel structural evaluation and rehabilitation design of an historic masonry fortress. *J Build Eng* 2023;63:105379. <https://doi.org/10.1016/j.jobe.2022.105379>.
- Valente M, Milani G, Grande E, Formisano A. Historical masonry building aggregates: advanced numerical insight for an effective seismic assessment on two row housing compounds. *Eng Struct* 2019;190(February):360–79. <https://doi.org/10.1016/j.engstruct.2019.04.025>.
- Formisano A, Ademovic N. An overview on seismic analysis of masonry building aggregates. *Front Built Environ* 2022;8(August):1–14. <https://doi.org/10.3389/fbuil.2022.966281>.
- Chieffo N, Formisano A, Lourenço PB. Seismic vulnerability procedures for historical masonry structural aggregates: analysis of the historical centre of Castelpoto (South Italy). *Structures* 2023;48(January):852–66. <https://doi.org/10.1016/j.istruc.2023.01.022>.
- Chácará C, Mendes N, Lourenço P. Simulation of shake table tests on out-of-plane masonry buildings. Part (IV): macro and micro FEM based approaches. *Int J Archit Herit* 2017;11(1):103–16. <https://doi.org/10.1080/15583058.2016.1238972>.
- Sharma S, Silva LC, Graziotti F, Magenes G, Milani G. Modelling the experimental seismic out-of-plane two-way bending response of unreinforced periodic masonry panels using a non-linear discrete homogenized strategy. *Eng Struct* 2021;242(June). doi: 10.1016/j.engstruct.2021.112524.
- Lourenço PB, Rots J. Multisurface interface model for analysis of masonry structures. *J Eng Mech* 1997;123(7):660–8.
- Abdulla KF, Cunningham LS, Gillie M. Simulating masonry wall behaviour using a simplified micro-model approach. *Eng Struct* 2017;151:349–65. <https://doi.org/10.1016/j.engstruct.2017.08.021>.
- D'Altri AM, de Miranda S, Castellazzi G, Sarhosis V. A 3D detailed micro-model for the in-plane and out-of-plane numerical analysis of masonry panels. *Comput Struct* 2018;206:18–30. <https://doi.org/10.1016/j.compstruc.2018.06.007>.
- Funari MF, Silva LC, Savalle N, Lourenço PB. A concurrent micro/macro FE-model optimized with a limit analysis tool for the assessment of dry-joint masonry structures. *Int J Multiscale Comput Eng* 2022;20(5):53–64. <https://doi.org/10.1615/intjMultCompEng.2021040212>.
- Lemos JV. Discrete element modeling of masonry structures. *Int J Archit Herit* 2007;1(2):190–213. <https://doi.org/10.1080/15583050601176868>.
- Psycharis IN, Drougas AE, Dasiou ME. Seismic behaviour of the walls of the Parthenon: a numerical study. In: *Computational methods in structural dynamics and earthquake engineering*; 2009. p. 265–83. <https://doi.org/10.1007/978-94-007-0053-612>.
- Sarhosis V, Asteris P, Wang T, Hu W, Han Y. On the stability of colonnade structural systems under static and dynamic loading conditions. *Bull Earthq Eng* 2016;14(4):1131–52. <https://doi.org/10.1007/s10518-016-9881-z>.
- Bui T, Limam A, Sarhosis V, Hjjaj M. Discrete element modelling of the in-plane and out-of-plane behaviour of dry-joint masonry wall constructions. *Eng Struct* 2017;136:277–94. <https://doi.org/10.1016/j.engstruct.2017.01.020>.
- Bui TT, Limam A, Sarhosis V. Failure analysis of masonry wall panels subjected to in-plane and out-of-plane loading using the discrete element method. *Eur J Environ Civ Eng* 2021;25(5):876–92. <https://doi.org/10.1080/19648189.2018.1552897>.
- Sarhosis V, Garrity SW, Sheng Y. Influence of brick-mortar interface on the mechanical behaviour of low bond strength masonry brickwork lintels. *Eng Struct* 2015;88:1–11. <https://doi.org/10.1016/j.engstruct.2014.12.014>.
- Sarhosis V, Sheng Y. Identification of material parameters for low bond strength masonry. *Eng Struct* 2014;60:100–10. <https://doi.org/10.1016/j.engstruct.2013.12.013>.
- Savalle N, Lourenço PB, Milani G. Joint stiffness influence on the first-order seismic capacity of dry-joint masonry structures: numerical DEM investigations. *Appl Sci* 2022;12(4). <https://doi.org/10.3390/app12042108>.
- Ferrante A, Giordano E, Clementi F, Milani G, Formisano A. Fe vs. De modeling for the nonlinear dynamics of a historic church in central Italy. *Geosciences* 2021;11(5):1–20. <https://doi.org/10.3390/geosciences11050189>.
- Schiavoni M, Giordano E, Roscini F, Clementi F. Numerical assessment of interacting structural units on the seismic damage: a comparative analysis with different modeling approaches. *Appl Sci* 2023;13(2). <https://doi.org/10.3390/app13020972>.
- Cattari S, Calderoni B, Caliò I, Camata G, de Miranda S, Magenes G, et al. *Nonlinear modeling of the seismic response of masonry structures: critical review and open issues towards engineering practice*, Vol. 20, no. 4. Netherlands: Springer; 2022.



- [37] Displacement method Analyzer. User's Manual, release 10.2. Delft (Netherlands): DIANA FEA BV; 2017.
- [38] Itasca. Three dimensional distinct element code (3DEC), Version 7.0. Official Documentation. Minneapolis, USA: Itasca Consulting Group; 2019.
- [39] Martins L., Vasconcelos G., Ortega J., Lourenço P.B., Rodrigues H., Silva L., et al. Characterization of dry stone walls to out-of-plane actions. 10 Congresso Nacional de Mecânica Experimental. Lisbon; 2016.
- [40] Maccarini H, Vasconcelos G, Rodrigues H, Ortega J, Lourenço PB. Out-of-plane behavior of stone masonry walls: experimental and numerical analysis. *Constr Build Mater* 2018;179:430–52. <https://doi.org/10.1016/j.conbuildmat.2018.05.216>.
- [41] Murano A, Ortega J, Vasconcelos G, Rodrigues H. Influence of traditional earthquake-resistant techniques on the out-of-plane behaviour of stone masonry walls: experimental and numerical assessment. *Eng Struct* 2019;201:109815. <https://doi.org/10.1016/j.engstruct.2019.109815>.
- [42] Roca P, Cervera M, Gariup G, Pelà L. Structural analysis of masonry historical constructions. Classical and advanced approaches. *Arch Comput Methods Eng* 2010;17(3):299–325. <https://doi.org/10.1007/s11831-010-9046-1>.
- [43] Panagiotis A, Plevris V, Sarhosis V, Papaloizou L, Mohebbkhan A, Komodromos P, et al. Numerical modeling of historic masonry structures. In: Panagiotis A, editor. *Handbook of research on seismic assessment and rehabilitation of historic structures*. Hershey, PA (USA): IGI Global; 2015. p. 213–55.
- [44] Bartoli G, Betti M. A numerical study on seismic risk assessment of historic masonry towers: a case study in San Gimignano. *Bull Earthq Eng* 2016. <https://doi.org/10.1007/s10518-016-9892-9>.
- [45] Betti M, Vignoli A. Numerical assessment of the static and seismic behaviour of the basilica of Santa Maria all'Impruneta (Italy). *Constr Build Mater* 2011;25(12):4308–24. <https://doi.org/10.1016/j.conbuildmat.2010.12.028>.
- [46] Tiberti S, Acito M, Milani G. Comprehensive FE numerical insight into Finale Emilia Castle behavior under 2012 Emilia Romagna seismic sequence: Damage causes and seismic vulnerability mitigation hypothesis. *Eng Struct* 2016;117:397–421. <https://doi.org/10.1016/j.engstruct.2016.02.048>.
- [47] Maccarini H, Vasconcelos G, Rodrigues H, Ortega J, Lourenço P. Out-of-plane behaviour of stone masonry walls: experimental and numerical analysis. *Constr Build Mater* 2017;179:430–52. <https://doi.org/10.1016/j.cois.2017.06.009>.
- [48] Murano A, Ortega J, Vasconcelos G, Rodrigues H. Influence of traditional earthquake-resistant techniques on the out-of-plane behaviour of stone masonry walls: experimental and numerical assessment. *Eng Struct* 2019;201(October):109815. <https://doi.org/10.1016/j.engstruct.2019.109815>.
- [49] Lemos J, Campos Costa A. Simulation of shake table tests on out-of-plane masonry buildings. Part (V): discrete element approach. *Int J Archit Herit* 2017;11(1):117–24. <https://doi.org/10.1080/15583058.2016.1237587>.
- [50] Mirabella Roberti G., Spina O. Discrete element analysis on the Sardinian 'Nuraghe'. Proceedings of the Historical Constructions Conference, Guimarães (Portugal) 2001; pp. 719–728.
- [51] Tóth AR, Orbán Z, Bagi K. Discrete element analysis of a stone masonry arch. *Mech Res Commun* 2009;36(4):469–80. <https://doi.org/10.1016/j.mechrescom.2009.01.001>.
- [52] Mordanova A, de Felice G, Genoese A. Assessment of the stability condition of the Claudio aqueduct; 2017.
- [53] Gonen S, Pulatsu B, Erdogmus E, Karaesmen E, Karaesmen E. Quasi-static nonlinear seismic assessment of a fourth century A.D. Roman Aqueduct in Istanbul, Turkey. *Heritage* 2021;4(1):401–21. <https://doi.org/10.3390/heritage4010025>.
- [54] Papantonopoulos C, Psycharis IN, Papastamatiou DY, Lemos JV, Mouzakis HP. Numerical prediction of the earthquake response of classical columns using the distinct element method. *Earthq Eng Struct Dyn* 2002;31(9):1699–717. <https://doi.org/10.1002/eqe.185>.
- [55] Psycharis IN, Lemos JV, Papastamatiou DY, Zambas C, Papantonopoulos C. Numerical study of the seismic behaviour of a part of the Parthenon Pronaos. *Earthq Eng Struct Dyn* 2003;32(13):2063–84. <https://doi.org/10.1002/eqe.315>.
- [56] Lourenço PB, Gaetani A. *Finite element analysis for building assessment - advanced use and practical recommendations*. Abingdon (UK): Routledge; 2022.
- [57] Scacco J, Salazar G, Bianchini N, Mendes N, Cullimore C, Jain L. Seismic assessment of the church of Carmo Convent. In: Congress on numerical methods in engineering (CMN2019); 2019, no. July. p. 1–16.
- [58] Sincraian GE, Lemos JV. Seismic analysis of a stone masonry aqueduct using discrete elements. In: 8th Canadian conference on earthquake engineering; 1999. p. 131–6.
- [59] Drei A, Oliveira Sousa C. The seismic behaviour of the 'Aqueduto da Amoreira' in Elvas using distinct element modelling. In: Proceedings of the 3rd international seminar on historical constructions; 2001. p. 903–12.
- [60] Mirabella Roberti G, Spina O. Discrete element analysis on the Sardinian 'Nuraghe'. In: Proceedings of the 3rd International Seminar on Historical Constructions; 2001. p. 719–27.
- [61] de C. Oliveira DV, Grecchi G, McCall A, Noh J, Speer E, Tohidi M. Seismic analysis of the Roman Temple of Évora, Portugal; 2012. [Online]. Available: [https://repositorium.sdum.uminho.pt/bitstream/1822/22022/1/2012\\_Seismic\\_analysis\\_of\\_the\\_Roman\\_Temple\\_of\\_Évora\\_%2C\\_Portugal.pdf](https://repositorium.sdum.uminho.pt/bitstream/1822/22022/1/2012_Seismic_analysis_of_the_Roman_Temple_of_Évora_%2C_Portugal.pdf).
- [62] Rouxinol G., Morais M. Analysis of masonry arch bridges using DEM with two distinct mesh generations; 9th International Masonry Conference 2014, Guimarães (Portugal), 2014.
- [63] Lemos JV, Oliveira Sousa C, Navarro M. 3-D nonlinear behavior of an obelisk subjected to the Lorca May 11, 2011 strong motion record. *Eng Fail Anal* 2015;58:212–28. <https://doi.org/10.1016/j.engfailanal.2015.09.001>.
- [64] Pulatsu B, Erdogmus E, Bretas EM. Parametric study on masonry arches using 2D discrete-element modeling. *J Archit Eng* 2018;24(2). [https://doi.org/10.1061/\(asce\)jae.1943-5568.0000305](https://doi.org/10.1061/(asce)jae.1943-5568.0000305).
- [65] Pulatsu B, Gencer F, Erdogmus E. Study of the effect of construction techniques on the seismic capacity of ancient dry-joint masonry towers through DEM. *Eur. J. Environ. Civ. Eng* 2020. <https://doi.org/10.1080/19648189.2020.1824823>.
- [66] Oliveira Sousa C, Lemos JV, Sincraian GE. Modelling large displacements of structures damaged by earthquake motions. *Eur. Earthq. Eng* 2002;16(3):56–71.
- [67] Schlegel R., Rautenstrauch K. "Failure analysis of masonry shear walls," Numer. Model. Discret. Mater., Proceedings of the First International UDEC/3DEC Symposium, Bochum, Germany, 29 September - 1 October 2004, pp. 15–18.
- [68] Alexandris A, Protopapa E, Psycharis I. Collapse mechanisms of masonry buildings driven by the distinct element method; 2004.
- [69] de Felice G. Out-of-plane fragility of historic masonry walls; Proceedings of the Structural analysis of historical constructions Conference, Padova, Italy, 10-13 November 2004, pp. 1143–1148.
- [70] Sarhosis V, Oliveira DV, Lemos JV, Lourenço PB. The effect of skew angle on the mechanical behaviour of masonry arches. *Mech Res Commun* 2014;61:53–9. <https://doi.org/10.1016/j.mechrescom.2014.07.008>.
- [71] Gomes JP, Lemos JV. Characterization of the dynamic behavior of a concrete arch dam by means of forced vibration tests and numerical models. *Earthq Eng Struct Dyn* 2020;49(7):679–94. <https://doi.org/10.1002/eqe.3259>.
- [72] Ortega Heras J. *Reduction of the seismic vulnerability of vernacular architecture with traditional strengthening solutions*. University of Minho; 2018.